HHS Public Access

Author manuscript

Mol Cell. Author manuscript; available in PMC 2021 May 07.

Published in final edited form as:

Mol Cell. 2020 May 07; 78(3): 382–395.e8. doi:10.1016/j.molcel.2020.02.018.

N^6-Deoxyadenosine Methylation in Mammalian Mitochondrial DNA

Ziyang Hao[1,6], **Tong Wu**[1,6], **Xiaolong Cui**[1], **Pingping Zhu**[1,2], **Caiping Tan**[1,3], **Xiaoyang Dou**[1], **Kai-Wen Hsu**[4], **Yueh-Te Lin**[4], **Pei-Hua Peng**[4], **Lisheng Zhang**[1], **Yawei Gao**[1,5], **Lulu Hu**[1], **Hui-Lung Sun**[1], **Allen Zhu**[1], **Jianzhao Liu**[1], **Kou-Juey Wu**[4], **Chuan He**[1,7,*]

[1]Department of Chemistry, Department of Biochemistry and Molecular Biology, Institute for Biophysical Dynamics, Howard Hughes Medical Institute, The University of Chicago, 929 East 57th Street, Chicago, IL 60637, USA.

[2]School of Life Science, Zhengzhou University, Zhengzhou, 450001, China.

[3]MOE Key Laboratory of Bioinorganic and Synthetic Chemistry, School of Chemistry and Chemical Engineering, Sun Yat-sen University, Guangzhou 510275, China.

[4]Cancer Genome Research Center, Chang Gung Memorial Hospital at Linkou, Taoyuan 333, Taiwan.

[5]Clinical and Translational Research Center of Shanghai First Maternity and Infant Hospital, Shanghai Key Laboratory of Signaling and Disease Research, School of Life Sciences and Technology, Tongji University, Shanghai 200092, China.

[6]These authors contributed equally

[7]Lead contact

SUMMARY

N^6-methyldeoxyadenosine (6mA), has recently been shown to exist and play regulatory roles in eukaryotic genomic DNA. However, biological functions of 6mA in mammals have yet to be explored largely due to its low abundance in most mammalian genomes. Here, we report that mammalian mitochondrial DNA (mtDNA) is enriched for 6mA. The level of 6mA in HepG2 mtDNA is at least 1,300-fold higher than that in gDNA under normal growth conditions, corresponding to ~four 6mA modifications on each mtDNA molecule. METTL4, a putative mammalian methyltransferase, can mediate mtDNA 6mA methylation, which contributes to

*Correspondence: chuanhe@uchicago.edu (C.H).

AUTHOR CONTRIBUTIONS

C.H., H.Z. and T.W. conceived the idea and designed the experiments. H.Z. and T.W. performed most experiments. X.C. and X.D analyzed high-throughput sequencing data. P.Z., C.T., K-W.H., Y-T.L., P-H.P., L.Z., Y.G., L.H., H-L.S., A.Z., and J.L. provided assistance on experiments. K-J.W. provided important suggestions on experiment results and the manuscript. H.Z., T.W., and C.H. wrote the manuscript. H.Z. and T.W. contributed equally.

DECLARATION OF INTERESTS

C.H. is a scientific founder and a scientific advisory board member of Accent Therapeutics. Inc. and a shareholder of Epican Genentech.

attenuated mtDNA transcription and reduced mtDNA copy number. Mechanistically, the presence of 6mA could repress mitochondrial transcription factor (TFAM) binding and TFAM-dependent DNA bending. Under hypoxia, the 6mA level in mtDNA could be further elevated, suggesting regulatory roles of 6mA in mitochondrial stress response. Our study reveals DNA 6mA as a regulatory mark in mammalian mtDNA.

eTOC BLURB

Hao et al. showed that N^6-methyldeoxyadenosine (6mA) modification is notably enriched in human mitochondria DNA and regulates mitochondrial transcription, replication, and activity.

INTRODUCTION

DNA methylation is a widespread epigenetic mechanism that plays critical roles in a wide range of biological processes (Jones and Takai, 2001). 5-methylcytosine (5mC) is predominantly found in higher eukaryotes (Ehrlich and Wang, 1981), especially in plants (Zhang et al., 2006) and mammals (Chen and Riggs, 2011). In contrast, N^6-methyldeoxyadenosine (6mA) is widespread in prokaryotes and functions primarily in restriction–modification (R-M) systems (Luo et al., 2015; Wion and Casadesus, 2006). As there is no equivalent bacterial restriction–modification system found in eukaryotes, the distributions and biological functions of 6mA in eukaryotic genomic DNA (gDNA) had, until recently, remained elusive. Recent studies uncovered the genome-wide distribution and potential regulatory roles of 6mA in the genomes of *Chlamydomonas reinhardtii* (Fu et al., 2015), ciliates (Beh et al., 2019; Luo et al., 2018), *Caenorhabditis elegans* (Greer et al., 2015), *Drosophila* (Zhang et al., 2015), and fungi (Mondo et al., 2017), indicating the presence of 6mA as an alternative DNA base methylation besides 5mC in eukaryotes.

In *C. reinhardtii*, 6mA is present in over 14,000 genes and exhibits a periodic distribution pattern near transcription start sites (TSSs), implying a possible role in nucleosome positioning and gene activation (Fu et al., 2015). In *Tetrahymena* and *Oxytricha*, 6mA on DNA disfavors nucleosome wrapping and plays a role in chromatin organization (Luo et al., 2018; Beh et al., 2019). In fungi, 6mA is concentrated around the TSSs and occurs symmetrically at ApT dinucleotides (Mondo et al., 2017). In *C. elegans* and *Drosophila*, 6mA may affect trans-generational inheritance and is found in certain transposons (Greer et al., 2015; Zhang et al., 2015).

While the levels of 6mA in genomes of certain invertebrates is relatively high, 6mA levels in the genomes of vertebrates and mammals tend to be low, ranging from a few to tens of ppm of the total deoxyadenosines, to even lower levels under normal growth conditions (Koziol et al., 2016; Schiffers et al., 2017; Wu et al., 2016). Nevertheless, potential roles of DNA 6mA in vertebrates and mammalian cells have been proposed (Koziol et al., 2016; Wu et al., 2016; Xie et al., 2018, Yao et al., 2017). In mouse embryonic stem cells, 6mA was enriched in young and active LINE1 transposons on the X chromosome at the frequency of 25–30 ppm of deoxyadenine (Wu et al., 2016). In glioblastoma cancer stem cells and patient tumors, 6mA was found as a repressive maker, which associates with repressive histone mark H3K9me3 in genes related with neurogenesis and neuronal development. 6mA was also

shown to play roles in stress response, including chronic restraint stress response in mouse brain (Yao et al., 2017) and mitochondrial stress adaptation in *C. elegans* (Ma et al., 2019).

We have speculated that 6mA could accumulate temporally and/or spatially in DNA regions to complement functional roles of the predominant 5mC marks in mammals (Luo and He, 2017). While the presence of potential roles of 6mA in mammalian genomic DNA remain to be investigated, we report here that mitochondrial DNA (mtDNA) is enriched for 6mA. Within the same cells, the level of 6mA in mtDNA can be at least 1300-fold higher than that in total DNA, particularly under certain stress conditions. The presence of 6mA markedly attenuates transcription activity of the mitochondrial transcription complex *in vitro* and therefore results in reduced transcription in human mitochondria. We show that METTL4, a putative mammalian methyltransferase which closely homologous to the RNA N^6-methyladenosine (m^6A) methyltransferases METTL3-METTL14 (Liu et al., 2014), can catalyze 6mA mtDNA methylation, contributing to the attenuation of mtDNA transcription and the reduction of mtDNA copy number. Mechanistically, the presence of 6mA could repress mitochondrial transcription factor (TFAM) binding and TFAM-dependent DNA bending. Under hypoxia, the 6mA level in mtDNA could be further elevated compared with that under homeostatic conditions, suggesting 6mA as a regulatory mark in mammalian mtDNA. Taken together, we have discovered 6mA as a dynamic mtDNA mark that affects gene expression regulation of the human mitochondrial genome.

RESULTS

6mA in Human Mitochondrial DNA

We hypothesized that 6mA could be enriched in specific subcellular locations and exert certain functions. To test this hypothesis, we quantified 6mA level in total genomic DNA (gDNA) and in purified mtDNA (isolated from the same HepG2 cells) via ultra-performance liquid chromatographytandem mass spectrometry (UHPLC-QQQ-MS/MS). We ensured that the HepG2 cells used for our experiments were not contaminated with mycoplasma DNA (Figure S1A), which could contain 6mA (Lluch-Senar et al., 2013). Consistent with a previous study (Schiffers et al., 2017), we detected a low level (up to ~0.3 ppm, approximately the detection limit of our current UHPLC-QQQ-MS/MS) of 6mA/dA in HepG2 gDNA, using careful calibrations and a mock control (Figures 1A and S1B, C). Crude mtDNA was extracted from intact mitochondria which was isolated by utilizing a commercially available kit. This method yields a ~6-fold enrichment of mtDNA over total DNA by RT-qPCR (Quispe-Tintaya et al., 2013), resulting in a 6mA/dA level at ~20 ppm, a more than 60-fold enrichment over that in HepG2 gDNA (Figures 1A and S1D). To further eliminate gDNA contamination and enrich mtDNA, a circular DNA-safe DNase, which digests most linear chromosomal DNA but not circular mtDNA, was applied. After digestion, mtDNA was more than 100-fold enriched over total DNA by RT-qPCR with the 6mA/dA level reaching ~400 ppm (Figures 1A and S1D), representing a more than 1,300-fold enrichment than that in gDNA and corresponding to approximately four 6mA modifications per mtDNA molecule.

Note that even after DNase digestion, there is still residual nuclear DNA contamination left (Gould et al., 2015). Our approach yields mtDNA accounting for ~43% of total mapped

reads from DNA sequencing in the “purified” mtDNA pool (Figure S1E), which exceeds the highest mtDNA enrichment level obtained in murine cell lines (MEFs, 22.5%) (Quispe-Tintaya et al., 2013) and lymphoblastoid cell lines (COLO 829BL, 34.6%) (Gould et al., 2015) reported so far. The real content of 6mA in mtDNA should be even higher if future approaches are developed to further improve mtDNA enrichment. The same approach was applied to quantify 6mA level in gDNA and mtDNA in MDA-MB-231 cells, 143B cells, mouse primary fibroblast cells, testes, and spleen. 6mA was shown to be enriched in mtDNA for all these tested cell lines and tissues (Figures 1B and S2A).

We then performed dot blot analysis using an anti-6mA-specific antibody to demonstrate the existence of 6mA in mtDNA. The specificity of this 6mA antibody was validated with 6mA signals detected only in the 6mA-containing probe but not in the 6mA-free probe (Figure S2B). Using the same antibody, we detected 6mA signals only with endogenous mtDNA, but not with total DNA or PCR-amplified mtDNA (Figure 1C). The existence of 6mA in mtDNA was further supported by immunofluorescence staining. As the 6mA antibody also recognizes RNA m^6A modification (Figure 1D), stringent RNase treatment was applied to completely remove signals derived from endogenous RNA. After RNase treatment, 6mA signals (green) in HepG2 cells co-localized with mitochondria marked by MitoTracker (red), with weak to no visible signal detected in the nucleus (Figure 1D). In addition, we did not detect 6mA signals in DNase- and RNase-treated HepG2 cells. We repeated the imaging experiment by using rho zero 143B cells, a human osteosarcoma cell line depleted of mtDNA (King and Attardi, 1989). Upon RNase treatment, 6mA signals (green) overlap well with MitoTracker (red) in normal 143B cells, with no 6mA signals detected in rho zero cells, confirming that the signals detected in 143B cells were indeed derived from mtDNA (Figure S2C). Altogether, these data strongly indicate that human mtDNA contains enriched 6mA.

We next sought to map 6mA distribution in mtDNA and to identify potential consensus methylation motifs. Considering the small size of human mitochondrial genome (16,569 base pair length), we employed a photo-crosslinking, enzyme digestion and immunoprecipitation-based 6mA-mapping approach (Rossi et al., 2018), namely 6mA ChIP-exo, to map 6mA in mtDNA at a relatively high resolution (Figure 2A) using two different anti-6mA antibodies from two different companies (Synaptic Systems and NEB).

Nuclear mitochondrial DNA segment (NUMTs) were filtered out in the analysis to guarantee that the reads exclusively mapped to mtDNA but not nuclear DNA. Metagene profile depicts a successful 6mA enrichment (Figure S2D). Our 6mA-mapping results revealed 23 high-confidence 6mA modification sites ($p < 0.01$) that were not only distributed in the promoter region of mtDNA, but also clustered in ND2, COI, and ND4-6 regions (Figure 2B and 2C, left). A consensus sequence of CTTATC was discovered in these 6mA-enriched sites (Figure S2E), suggesting a potential sequence preference of the mtDNA 6mA modification. Peaks discovered by two different antibodies overlapped very well (Figures 2B and 2C). Correlation analysis between libraries generated by these two different antibodies showed strong positive correlation (spearman $r = 0.76$) (Figure 2D), validating the robustness of this 6mA-mapping approach.

The same 6mA-mapping method was applied to PCR-amplified 6mA-free mtDNA. We failed to obtain sufficiently enriched DNA for library construction, implying the presence of 6mA is critical for the successful enrichment using this antibody. 6mA-IP qPCR was performed to validate 6mA sites identified by 6mA-mapping. We examined 6 sites among 23 identified 6mA sites and three 6mA-negtive sites. The qPCR results showed ~3 to 5-fold enrichment on all selected 6mA-containing sites compared to 6mA-negative sites (Figure 2E).

METTL4 Accumulates in Mitochondria and Mediates 6mA Methylation in mtDNA

Three closely homologous members of the MTA70 family eukaryotic methyltransferases exist in mammals, namely, METTL3, METTL14, and METTL4 (Figures 3A and S3A, B), which are thought to have evolved from the MunI-like bacterial DNA 6mA methyltransferases (Iyer et al., 2016; Luo et al., 2015). METTL3 and METTL14 form a heterodimer complex to mediate mammalian m^6A mRNA methylation (Liu et al., 2014; Roundtree et al., 2017; Wang et al., 2016a; Wang et al., 2016b). The third member, METTL4, is also a homologue of the DNA 6mA methyltransferase DAMT-1 found in *C. elegans* (Figures S3A and S3B), and was proposed as a potential candidate for mammalian DNA 6mA methylation (Luo and He, 2017).

We performed immunofluorescence with an anti-METTL4 antibody and observed co-localization of METTL4 with MitoTracker in HepG2 and HeLa cells, indicating a substantial accumulation of METTL4 in mitochondria (Figure 3B). This observation is consistent with the public data in Human Protein Atlas (Atlas Antibodies Cat#HPA040061, RRID: AB_10697713), showing similar mitochondrial accumulation of METTL4. We also applied immunofluorescence in mouse tissues including brain, testis, liver and fat with two antibodies (HPA040061 from Sigma-Alrich and AP10377B from Abcepta) produced by using the N terminal and C-terminal immunogen sequences, respectively. The results consistently showed that METTL4 co-localizes with mitochondria in all tested tissues (Figure S3C). To verify this observation, we further examined METTL4 distribution in different subcellular fractions by western blot and found that METTL4 is significantly enriched in the mitochondrial fraction, with a very small portion found in fractions of the cytosol and nucleus (Figures 3C and S3D). To better examine the location of METTL4 inside mitochondria, we performed METTL4 immunoelectron microscopy in HepG2 cells and mouse testis (which have relatively high METTL4 expression) to investigate its sub-mitochondrial localization. METTL4 is shown to reside in the mitochondrial matrix, where mtDNA is located (Figure S3E). We next employed mitochondrial signal sequence-searching tools (MitoProt II and TargetP) to analyze METTL4 sequence, which showed that METTL4 has a low score in N-terminal mitochondrial targeting sequence (MTS) prediction. However, the recently developed Integrated Mitochondrial Protein Index (IMPI) (Smith and Robinson, 2018), which integrates the multiple datasets and machine learning algorithm, shows a high possibility of METTL4 to be a mitochondrial protein (IMPI score: 0.748).

Next, we evaluated the relationship between METTL4 and 6mA. We knocked down METTL4 in HepG2 cells and observed a 30% decrease of the 6mA/dA ratio in the mtDNA compared to the control (Figures 3D, S4A and S4B). Previous results showed that

knockdown of METTL4 did not change the RNA m^6A level in mRNA (Liu et al., 2014; Wang et al., 2014). We isolated different mitochondrial RNA species and showed that METTL4 knockdown has no significant effect on m^6A nor m^6Am levels for mitochondrial rRNAs, mRNAs and small RNAs (Figure 3E and S4C), suggesting that METTL4 acts on mtDNA rather than on mitochondrial RNAs. We then cloned, expressed and purified full-length human METTL4 (~53 kDa, Figure S4D) and a mutant METTL4 from HEK293T cells with the conserved methylation signature motif DPPW mutated to APPA. We incubated recombinant METTL4 proteins with isolated mtDNA in the presence of *S*-(5'-adenosyl)-L-methionine-d_3 (d_3-SAM), a deuterium-substituted methyl donor cofactor, and quantified d_3-6mA level using UHPLC-QQQ-MS/MS. We detected 6mA methyltransferase activity on both single-stranded and double-stranded mtDNA using wild-type METTL4 but not for the mutant (Figures 3F and 3G), with its activity on single-stranded DNA much higher. To verify the METTL4-mediated alteration of the 6mA modification on mtDNA, 6mA-IP qPCR of the 6mA-containing and 6mA-negative sites (revealed by 6mA ChIP-exo) were also performed in METTL4 knockdown and METTL4 overexpression cell lines, respectively. The enrichment fold of 6mA-containing sites decreased by ~30 to 40% in METTL4 knockdown cells compared with control cells. These sites were ~1.5-fold more enriched in METTL4 overexpressed cells. No such change was observed on 6mA-negative sites (Figures 3H and 3I). Taken together, we concluded that METTL4 can act as a methyltransferase to perform the 6mA methylation on mtDNA.

METTL4 Affects Mitochondrial Activity

The identification of METTL4 as a 6mA methyltransferase allowed us to probe the roles of 6mA in mammalian mitochondria. As mitochondria produce energy for the cell mainly through mitochondrial respiration and glycolysis, we performed a cell energy phenotype test which simultaneously reports mitochondrial respiration (oxygen consumption rate, OCR) and glycolytic activity (extracellular acidification rate, ECAR) to uncover how METTL4 affects cell energy production and utilization under basal and stressed conditions. Compared to the control cells, the knockdown of METTL4 exhibited elevated baseline activity (open squares) as well as increased mitochondrial respiration and glycolysis in response to mitochondrial stressors (closed squares) (Figures 4A and S4E, F). Thus, METTL4 appears to negatively affect mitochondrial activity under both basal and stressed (high-energy consuming) conditions. The same assay was also performed on rho zero 143B cells. Because rho zero cells lack mtDNA, they also lack mitochondrial components of oxidative phosphorylation (OXPHOS) complexes and, therefore, have very low OCR (Figures S4G and S4H). In contrast to HepG2 cells, no significant metabolic phenotype change was observed after METTL4 knockdown (Figures S4G-I) in rho zero cells, suggesting that METTL4 modulates mitochondrial activity through its function on mtDNA.

To study the mechanism of increased mitochondrial activity upon METTL4 knockdown, we examined the levels of OXPHOS complex components in control and METTL4 knockdown cells. The OXPHOS system is composed of five protein-lipid enzyme complexes,(Hatefi, 1985; Saraste, 1999), which is regulated by both mtDNA and nuclear genome (Reinecke et al., 2009). We observed an increase in OXPHOS complex III component and a slight increase of complex IV component in METTL4 knockdown cells compared to the control

(Figure 4B), which explains the elevated OCR observed upon METTL4 knockdown (Figures 4A, S4E and S4F).

As high mitochondrial OXPHOS activity may increase the level of cellular reactive oxygen species (ROS) (Bleier and Dröse, 2013; Guzy et al., 2005), and complex III is the primary site for ROS generation in mitochondria (Chen et al., 2003), we also monitored the effect of METTL4 on mitochondrial ROS levels using MitoTracker CM-H2XROS, a well-tested dye for ROS-specific staining in mitochondria (Degli Esposti, 2002). A time-lapse of fluorescence revealed increased ROS levels in the METTL4 knockdown cells compared to the control (Figure 4C). We then analyzed the effect of METTL4 on mitochondrial membrane potential ($\Delta\psi m$) by flow cytometry. Both scatter plots and histogram showed that the knockdown of METTL4 induced the hyperpolarization of $\Delta\psi_m$ (Figure 4D), which is consistent with its effect on ROS generation and mitochondrial respiration (Murphy, 2009). Taken together, our results show that the presence of METTL4 suppresses mitochondrial activity. The imbalanced mitochondrial activity induced by METTL4 knockdown leads to mitochondrial dysfunction and reduced cell proliferation (Figure 4E). The level of SDHA, a commonly used housekeeping mitochondrial marker, between control and METTL4 knockdown cells are similar (Figure S4J), indicating the aforementioned phenotypes were not due to increased mitochondria number when knocking down METTL4.

METTL4 Modulates Mitochondrial Transcripts Level and mtDNA Copy Number

To uncover the molecular mechanism underlying the role of METTL4 in mitochondrial function, we investigated the relationship between 6mA and mitochondrial gene expression. Both RNA-seq and RT-qPCR results shown an upregulation of mitochondrial rRNAs and most mRNAs upon METTL4 knockdown (Figures 5A and S5A), which could contribute to increased expression of OXPHOS complex components and upregulated mitochondrial activity.

We further performed rescue experiments to validate the effect of 6mA on mitochondrial gene expression. Overexpression of the wild-type METTL4, but not of the catalytically inactive METTL4 mutant (D292A, W294A), decreased mitochondrial mRNA levels in METTL4 stable knockdown cells (Figure 5B). We also examined the TFAM protein and mRNA level in METTL4 knockdown and control cells, with no obvious changes observed using real-time qPCR and western blot (Figure S5B). METTL4 knockdown appears to affect the level of each mitochondrial transcript to different extent, potentially due to additional post-transcriptional processing which largely determines individual mitochondrial transcript levels (Mercer et al., 2011).

We next analyzed levels of mitochondrial nascent polycistronic precursor RNAs instead of steady-state RNAs, which allows us to reveal the role of METTL4 on mitochondrial transcription without perturbations from ongoing endonucleolytic cleavage (splicing) and post-transcriptional modifications. Both the control and METTL4 knockdown HepG2 cells were labeled with 5’-ethynyluridine (5-EU) for 10, 20, 30 and 60 min, respectively. 5-EU-labeled RNAs were enriched for RT-qPCR analysis, with primers designed to span the splice junctions of mitochondrial nascent polycistronic RNAs, to ensure that only polycistronic precursor RNAs can be amplified. The normalized time curve showed a faster accumulation

rate of polycistronic transcripts upon METTL4 knockdown (Figures 5C and 5D), indicating that METTL4 is directly involved in mtDNA transcription regulation. We further discovered that the mtDNA copy number was elevated by ~2- fold in METTL4 knockdown cells relative to control cells (Figure 5E). Therefore, we hypothesized that the presence of mtDNA 6mA could affect mitochondrial transcription and replication, which are coupled in mitochondria (Agaronyan et al., 2015; Bonawitz et al., 2006).

6mA Suppresses Mitochondrial Transcription *in vitro*

Based on the 6mA-mapping results, we observed a notable 6mA peak locating at the promoter region (HSP and LSP) (Figure 2B and 2C, left), which was further validated by RT-qPCR (Figure 3H and 3I). To investigate whether 6mA at the promotor region could affect transcription initiation, we performed an *in vitro* transcription assay using linear transcription templates with or without one 6mA modification inserted at a specific site on HSP and LSP promoters (Figure S5C, Table S4). 6mA modifications at heavy-strand promoter (HSP) and light-strand promoter (LSP) were found to attenuate transcription by ~60% and 30%, respectively (Figures 6A, 6B and S5D). Transcripts generated from the light-strand promoter (LSP) were also decreased by ~30% in the 6mA-containing template (Figure S5D). No visible transcript was observed in transcription reactions (both HSP and LSP) in the absence of TFAM (Figures 6 A and S5D), confirming the specificity of the *in vitro* transcription assay. These results support a transcription suppression role of 6mA at mitochondrial promoter region.

Previous studies revealed that 6mA methylation could affect DNA bending (Bang et al., 2008; Fazakerley et al., 1989) and DNA-protein recognition (Polaczek et al., 1998). The key mitochondrial transcription unit TFAM is known to bind and bend mtDNA, and it bends mtDNA differently at LSP and HSP, which is thought to result in different *in vitro* transcription outcomes (Bestwick and Shadel; Uchida et al., 2017). We hypothesize that the presence of 6mA could either disrupt TFAM binding/bending or cause stalling/pausing of the transcription machinery by altering the physical properties of the template DNA or destabilizing the base-pairing between the DNA template and UTP (Wang et al., 2017).

6mA Affects DNA Binding and Bending by TFAM

To test our hypothesis, we performed an *in vitro* pull-down assay to investigate whether 6mA affects TFAM binding to mtDNA. 6mA-modified and unmodified HSP probes (Table S4) were mixed at 1:1 ratio. Purified His-tagged TFAM protein was incubated with this mixture followed by separation using Ni magnetic beads. LC-MS/MS showed that TFAM preferentially binds to the unmodified HSP probe (Figure 6C), indicating that 6mA impedes TFAM binding. We also performed EMSA using these 6mA modified or unmodified HSP probes. The presence of 6mA decreased the binding affinity of TFAM to its cognate DNA (Figures 6D and 6E). Interestingly, this attenuated binding effect was not detected when LSP probe was applied in the *in vitro* competition binding assay and EMSA (Figure S5E-G), which is consistent with the *in vitro* transcription results.

The presence of 6mA is reported to rigidify duplex DNA (Luo et al., 2018), thus disrupting of the bending of DNA by TFAM. We employed a Forster resonance energy transfer (FRET)

assay to test if 6mA could interrupt the bending of DNA by TFAM. Cy3 (donor) and Cy5 (acceptor) were labeled on two opposite ends of short HSP and LSP probes with or without 6mA (Table S4). The addition of 200 nM TFAM (binding saturates at 100 nM as shown by EMSA) led to bending of DNA probes and strong FRET signal. The presence of 6mA in the DNA probes prevented DNA bending by TFAM, as shown by ~22% and ~8% decreased FRET efficiency in HSP and LSP probes, respectively, compared to their unmodified counterparts (Figures 6F and S5H). Taken together, 6mA attenuates TFAM binding and bending of its cognate DNA. Because TFAM is also known to bend DNA outside the promoter regions (Ngo et al., 2011), this attenuation effect is not only relevant to transcription activation, but also mtDNA packaging and stability (Campbell et al., 2012; Lezza, 2012). Because TFAM is known to play critical roles in regulating mitochondrial replication and the structure of nucleoid (Campbell et al., 2012; Farge et al., 2014; Lezza, 2012), the presence of 6mA and its effect on TFAM may also impact mtDNA replication.

The mtDNA 6mA Level is Significantly Elevated under Hypoxic Stress

As the presence of 6mA could attenuate gene expression in mitochondria, we hypothesized that 6mA level in cells may be kept low in order to maintain proper mitochondrial function under normal conditions, but can be elevated under certain stress conditions to suppress mitochondrial activity. We discovered that the 6mA/dA level in mtDNA gradually increased and reached 0.1% (~3 fold higher compared with that in nomoxia) after 48 hr treatment, which corresponds to ~12 or more 6mA modifications per mtDNA molecule (Figure 7A).

We then compared the METTL4 level under normoxia and hypoxia. Both RT-qPCR and western blot showed upregulation of METTL4 upon hypoxia treatment (Figure 7B and S6A). Therefore, hypoxia could activate the expression of METTL4 within mitochondria to facilitate 6mA methylation. We then exposed METTL4 knockdown cells and control cells to hypoxia for 48 h. The 6mA level was ~70% lower in METTL4 knockdown cells than that in control cells (Figure 7C), confirming a key role of METTL4 in tuning the 6mA level in mtDNA under hypoxia. Since hypoxia-inducible factor-1α (HIF1α) is activated by hypoxia (Semenza, 2012) and hypoxia induces METTL4 expression (Figure S6A), we tested whether HIF-1α could regulate METTL4 expression and further affect mtDNA transcription. Constitutively active HIF1α (HIF1α-ΔODD) overexpression led to upregulated METTL4 expression (Figure S6B) and reduced mitochondrial transcript levels in control HepG2 cells, but showed no effect on mitochondrial transcripts in METTL4 knockdown cells (Figure S6C). The activation of the HIF1α-METTL4 axis under hypoxia could help cells to adapt to hypoxic stress through balancing increased ROS production (Fuhrmann and Brune, 2017).

We next performed 6mA-mapping in hypoxia-treated (48 hr) cells and uncovered 34 potential 6mA sites, with 21 sites (62%) overlapping with normoxia 6mA sites (Figures 7D, 7E, S6D, and S6E). We used two different 6mA antibodies and found a strong positive correlation (spearman r = 0.844, Figure S6F) between libraries generated from these antibodies. Although many 6mA sites appear to be conserved, there are also a number of 6mA sites that change under hypoxia, suggesting potential dynamics of 6mA methylation under different physiological conditions to affect gene expression. The introduction of 6mA

into mtDNA could be a mechanism for cells to cope with certain types of stresses, which will be important to explore in future studies.

DISCUSSION

Epigenetic modifications expand DNA information contents beyond the four canonical nucleotides and play critical roles in gene expression regulation (Bird, 2007). 5mC is the major epigenetic mark in vertebrates, exerting a predominant role in epigenetic inheritance, affecting transcription regulation, and is dynamically tuned by several identified methyltransferases, demethylases and reader proteins (Baubec and Schübeler, 2014; Maunakea et al., 2010; Weber et al., 2007; Wu and Zhang, 2013).

6mA in Mitochondrial DNA

Compared to 5mC, 6mA is prevalent in bacteria, playing critical roles in R-M systems but also in DNA replication, DNA repair and transcription regulation. Recent studies uncovered the presence and distribution of 6mA in eukaryotic genomes, which has shed lights on the potential functions of 6mA in diverse eukaryotes (Fu et al., 2015; Greer et al., 2015; Koziol et al., 2016; Liu et al., 2016; Mondo et al., 2017; Wu et al., 2016; Zhang et al., 2015). We discovered here enriched 6mA in human mitochondria DNA and its function in repressing the mitochondrial gene expression. Mitochondria are thought to have bacterial ancestry, most likely from the α-proteobacteria (Gray, 2012), in which the CcrM family of DNA 6mA methyltransferases are widespread and play critical roles beyond restriction-modification (Wright et al., 1997). Although a variety of pathways and mechanisms exist to tune mitochondrial functions, our current work adds an adenosine-based DNA methylation as a regulatory marker in the mammalian mitochondrial genome, which might trace back to bacterial origins and is distinct from the predominant 5mC methylation in the nuclear genomes of mammals. We want to stress the importance of depleting genomic DNA contamination in all measurements of the levels of 6mA in mtDNA. The samples used for LC-MS/MS measurements must be submitted to high-throughput sequencing in order to confirm enrichment of mtDNA.

METTL4 Can Localize in Mitochondrion and Contribute to mtDNA 6mA Methylation

METTL4 accumulates in mitochondria in cell lines and mouse tissues we have studied, as was confirmed by immunofluorescent imaging (Figure 3B, S3C), western blot (Figure 3C), and immunoelectron microscopy (Figure S3E). Knockdown and overexpression of METTL4 caused changes of the total mitochondrial 6mA level and mitochondrial functions, indicating that METTL4 can localize in mitochondrial matrix and function as an mtDNA 6mA methyltransferase.

It was reported that more than 98% of mitochondrial proteins are made outside mitochondria and are subsequently imported into mitochondria; among them, a large proportion have no cleavable sequence but some of them have internal targeting segments (Pfanner and Geissler, 2001) or non-canonical MTSs (Li et al., 2010). We found neither obvious N-terminal MTS nor cleavable pre-sequence in METTL4. It is possible that METTL4 may have internal targeting signals or unique non-canonical MTS which could be recognized by mitochondrial

surface receptors and further translocated into mitochondria, as some other mitochondrial proteins do (Pfanner and Geissler, 2001; Wiedemann et al., 2004). It will be interesting to elucidate how METTL4 translocates into mitochondria in the future.

Although METTL4 can reside in mitochondria, we could not exclude that METTL4 has other cellular functions. A recent study reported that METTL4 acts as a methyltransferase to install internal m^6Am methylation on U2 small nuclear RNA (snRNA) in HEK293T cells, suggesting that METTL4 could play a nuclear role on RNA splicing regulation (Chen et al., 2020). A majority of METTL4 protein localize in mitochondria in cells studied in this work. We confirmed the U2 snRNA m^6Am methylation role of METTL4; however, METTL4 knockdown showed relatively minor effects on alternative splicing in our system (Figure S5I). The role of METTL4 seems to be context dependent. It affects mitochondrial activity when it localizes to mitochondria, when it resides mostly in nucleus, it may impact splicing.

DNA 6mA Methylation Attenuates Mitochondrial Transcription by Interrupting TFAM Binding/Bending of DNA

Whether mtDNA modifications affect mitochondrial gene expression has been a long-standing question in the field (van der Wijst and Rots, 2015). Here we conclude that 6mA could suppress mitochondrial transcription through disrupting TFAM binding. 6mA methylation occurs at the promoter region of human mtDNA. One 6mA incorporated into the HSP promoter could cause marked suppression of mitochondrial transcription *in vitro*. The 6mA modification at the HSP promoter showed more profound effects on transcription (~60% reduction) than that at the LSP promoter (~30% reduction). This could be due to different sensitivities of these promoters in response to DNA binding/bending caused by TFAM; the region 50 bp upstream of HSP transcription start site is known to be very sensitive to TFAM binding when compares with LSP regions (Uchida et al., 2017). Because 6mA reduces base pairing (Wang et al., 2017) and alters rigidity of the modified DNA (Luo et al., 2018), the presence of 6mA could introduce physical alterations of HSP and LSP promoters to affect their interactions with TFAM to different extents.

The effects of 6mA on transcription in mitochondrial may not be limited to promoters. 6mA modifications scattering around gene body could affect mtDNA compaction by interrupting the DNA binding/bending of TFAM, as shown by our *in vitro* pull-down, EMSA and FRET assays. Apart from initiating transcription, TFAM is also a major structural protein of mammalian mitochondrial nucleoid that coats the entire mtDNA and plays a histone-like role (Alam et al., 2003; Ngo et al., 2011). Small variations in the TFAM-to-mtDNA ratio could dramatically disrupts mtDNA packaging and the fraction of nucleoids that are involved in mtDNA transcription and/or replication (Farge et al., 2014; Kukat et al., 2015). How mtDNA compaction affects mitochondrial transcription is not fully understood. More detailed future studies are required to elucidate the exact roles of 6mA.

Although detailed mechanisms remain to be elucidated, current results indicate that the physiological levels of 6mA could elicit a notable inhibition effect on the binding or processing ability of key components of mitochondrial transcription machinery, which is known to couple with replication (Agaronyan et al., 2015; Bonawitz et al., 2006). Mitochondrion affects a variety of cellular activities. An mtDNA 6mA modification change

(for instance, an increase under hypoxia) could affect mitochondrial function and impact numerous pathways, providing a potentially regulatory mechanism of cellular processes.

In summary, our study showed the presence of 6mA in human mitochondrial DNA, and identified METTL4 as a mtDNA 6mA methyltransferase. We showed that the METTL4-mediated 6mA methylation regulates the mitochondrial transcription and mtDNA copy number, thereby influencing mitochondrial activity. The 6mA level substantially increased under hypoxia, implying that the 6mA level can be regulated by cells in response to environmental stresses (Yao et al., 2017). Our discovery presented here could stimulate a new paradigm of DNA 6mA methylation research in regulating mammalian mitochondrial gene expression (Figure 7F).

STAR METHODS

LEAD CONTACT AND MATERIALS AVAILABILITY

Further information and requests for resources should be directed to and will be fulfilled by the Lead Contact, Chuan He (chuanhe@uchicago.edu). All unique/stable reagents generated in this study are available from the Lead Contact with a completed Materials Transfer Agreement.

EXPERIMENT MODEL AND SUBJECT DETAILS

Cell culture—HeLa cells, HepG2 cells, MDA-MB-231cells and HEK293T cells were purchased from ATCC. HeLa cells were cultured in DMEM (Gibco 11965) supplemented with 10% (v/v) fetal bovine serum (Gibco), penicillin and streptomycin (Gibco) and grown at 37 °C with 5% CO_2. HepG2, HEK293T cells were cultured in DMEM (Gibco 11995) supplemented with 10% (v/v) fetal bovine serum (Gibco), penicillin and streptomycin (Gibco) and grown at 37 °C with 5% CO_2. 143B cells, Rho zero 143B cells are gift from Dr. Y. H. Wei. Hypoxia treated cells were incubated at 37 °C, 5% CO_2 and 2.3% O_2. Primary fibroblasts were isolated from postnatal 0-to 4-day-old wild-type mice. The skin tissue was isolated and cut into small pieces in PBS with penicillin and streptomycin. These pieces were attached to 10 cm FBS-coated dishes (one mouse for one dish) and cultured in medium containing DMEM supplemented with 10% FBS, 1mM L-glutamine, 100 IU/mL penicillin and streptomycin. Cells were grown at 37 °C in 5% CO_2. As a part of cell authentication, cell lines used in this study were examined by mycoplasma contamination test using LookOut Mycoplasma PCR Kit (Sigma, MP0035).

METHOD DETAILS

Plasmid construction—The pHA-HIF-1α ΔODD) expression construct was obtained from L. Eric Huang (Univ. of Utah). Recombinant METTL4 (Isoform 1, 472 aa) was cloned from commercial cDNA clones (Open Biosystems) into vector pCDH-CMV-MCS-T2A copGFP with the restriction sites EcoRI and NotI. Flag-tag was fused at the C-terminus of gene and generated by PCR amplification. The primers used for subcloning are listed in Table S4. The human TFAM gene was synthesized with codon optimization (Genscript) and cloned into the pET28a expression vector (Novagen) between the XhoI and BamHI sites. This construct encodes residues 43–246, which eliminating the N-terminal mitochondrial

leader sequence (residues 1–42). Plasmids with high purity were prepared with QIAGEN Plasmid Maxi kit (Qiagen), and transfected into HEK293T cell.

Expression and purification of recombinant human METTL4 protein—Plasmid harboring METTL4 was transfected into HEK293T cells following the manufacturer's protocol. Cells were grown at 37 °C with 5% CO_2 and harvested after 48 hr. To purify METTL4 protein, cells were suspended in 2 volumes of lysis buffer (150 mM KCl, 10 mM HEPES (pH 7.6), 2 mM EDTA, 0.5% NP-40, 0.5 mM DTT, protease inhibitor cocktail) followed by rotating at 4 °C for 30 min to lysis the cell completely. The lysate solution was centrifuged at 13000 rpm for 30 min at 4 °C. The resultant supernatant was passed through a 0.22 μm membrane syringe filter and then incubated with anti-Flag M2 magnetic beads (Sigma-Aldrich) at 4 °C on a rotate wheel for 3 hr. Afterwards, the protein-beads complex was washed with ice-cold B&W buffer (200 mM NaCl, 50 mM HEPES (pH 7.6), 2 mM EDTA, 0.05% NP-40, 0.5 mM DTT, protease inhibitor cocktail) and METTL4 protein was eluted twice by incubation with 300 μl elution buffer (200 mM KCl, 50 mM Tris-HCl pH 8.0, 1.5 mM $MgCl_2$, 0.5 mM DTT, 1× proteinase inhibitor cocktail, 0.5 mg/ml 3× Flag peptide (Genscript)) for 30 min at 4 °C. The protein was concentrated by using Amicon Ultra 10K centrifugal filter Device (Millipore).

Expression and purification of TFAM protein—Plasmid harboring TFAM gene was transformed into BL21 (DE3) Escherichia coli (Invitrogen). LB medium (20 mL) containing 50 μg/mL kanamycin was inoculated with a single colony and grown overnight at 37 °C. The overnight culture was diluted to 4 L LB medium and grown until an OD600 reached to 0.6. After induction with 1 mM isopropyl β-d-1-thiogalactopyranoside, the culture was grown overnight at room temperature (25 °C). The cells were harvested and resuspended in 60 ml lysis buffer (20 mM Tris-HCl, 500 mM NaCl, pH 7.5) and sonicated for 15 min (10 s on and 20 s off) on ice. After centrifugation for 30 min at 4 °C, His-tagged TFAM was purified from the supernatant with Histrap HP column (GE healthcare). The protein was eluted with elution buffer (20 mM Tris-HCl pH 7.5, 500 mM NaCl, 300 mM imidazole) and further purified by gel filtration chromatography using a Hi-Load Superdex 200 16/60 column (GE Healthcare) pre-equilibrated with running buffer (20 mM Tris-HCl pH 7.5, 300 mM NaCl, 1 mM DTT), in an FPLC (GE healthcare). The peak fraction was collected and concentrated using Amicon Ultra-15 concentrators (Millipore) with a molecular weight cutoff of 10 kDa. The protein was flash-frozen in liquid nitrogen with 15% glycerol and stored at −80 °C for further use.

Mitochondria isolation and gDNA/mtDNA extraction—Cells were harvested and washed once in isolation buffer (225 mM mannitol, 75 mM sucrose, 20 mM MOPS pH 7.2, 1 mM EGTA, 0.1% BSA). Cell pellets were then re-suspended and incubated in lysis buffer (100 mM sucrose, 10 mM MOPS pH 7.2, 1 mM EGTA, 0.1% BSA) for 5 min at 4 °C, and then homogenized with Omni homogenizer for 1 min at low speed. One volume of 1.25 M sucrose was then added, and the mixture was centrifuged at 1000 g for 10 min at 4 °C. The supernatant was transferred to a new tube, which was subjected to centrifuge at 12000 g for 5 min. The mitochondria-containing pellet was further purified by the Mitochondria Isolation kit (Miltenyi Biotec) according to manufacturer's protocol. The eluted

mitochondria were washed with high salt buffer (10 mM Tris-HCl pH 7.6, 10 mM KCl, 10 mM $MgCl_2$, 0.4 M NaCl and 2 mM EDTA) and then resuspended in plasmid-safe reaction buffer (33 mM Tris-acetate pH 7.5, 66 mM potassium acetate, 10 mM magnesium acetate and 1 mM DTT). mtDNA was extracted from mitochondria by vigorous vortex followed by 2-3 stokes with 27 ½ G needle. Plasmid-safe ATP-dependent DNase (Epicentre) was added according to manufacturer's protocol to digested contaminated nuclear DNA. The reaction was cleaned up by the DNA Clean & Concentrator kit (Zymo) to yield "pure" mitochondrial DNA.

Immunofluorescence microscopy—Around 2×10^4 HepG2, 143B or HeLa cells were seeded in Lab-Tec 8-well chamber (Thermo) and grown overnight at 37 °C, 5% CO_2. The next day, cells were stained with 300 nM MitoTracker Deep Red FM (Thermo Fisher) in DMEM medium for 30 min at 37 °C. After washing with cold PBS, cells were fixed in 4% paraformaldehyde and permeabilized with PBS containing 0.3% Triton X-100 at room temperature. The permeabilized cells were washed with PBS and then blocked for 1 hr in blocking buffer (1% BSA in PBS containing 0.1% Tween) containing either 50 μg/mL RNase A (Invitrogen) or 50 μg/mL RNase A plus 2 U/μL DNase I (Invitrogen) for RNA digestion or RNA/DNA elimination, respectively. After blocking, cells were then incubated in 6mA antibody (1: 1,000, Synaptic Systems) at 4 °C overnight and then in the secondary antibody (goat anti-rabbit IgG Alexa Fluor 488, Thermo Fisher) at a 1:2000 dilution. For METTL4 immunostaining, HepG2 and HeLa cells were treated similarly as 6mA immunostaining before incubated with anti-METTL4 antibody (Sigma, HPA040061, 1 μg/mL) at 4 °C overnight and then in the secondary antibody (goat anti-rabbit IgG Alexa Fluor 488, Thermo Fisher) at a 1:2000 dilution. Cells were stained with 1:1000 diluted DAPI (Thermo) before subjected to Leica SP5 II laser scanning confocal microscopy. The images were processed using ImageJ software.

Western Blotting—Cells were lysed in RIPA lysis buffer (150 mM NaCl, 1% NP-40, 0.5% sodium-deoxycholate, 0.1% sodium dodecyl sulfate, 10 mM Tris-HCl pH 8.0) at 4 °C for 30 min. Lysates were cleared by centrifuging at 15000 rpm for 15 min at 4 °C. Protein concentration from supernatants were measured by using Quick Start Bradford Protein Assay Kit (Bio-Rad) and equal amounts of protein (20-30 μg) were subjected to SDS-PAGE and transferred to nitrocellulose membrane (Bio-Rad). The membranes were then blocked for 30 min in 5% milk in PBST (0.1% Tween-20), which were further subject to an overnight incubation with primary antibodies in 5% milk in PBST (0.1% Tween-20) at 4 °C. On the second day, membranes were washed 5 times for 5 min each with PBST (0.1% Tween-20) and then incubated with secondary antibodies for 1 hr at room temperature. Membranes were washed 5 times for 5 min each with PBST (0.1% Tween-20) before applied with ECL and developed.

Dot blotting—Synthetic DNA probes, gDNA, mtDNA and PCR products (mixture of PCR product 1 and 2, primers listed in Table S4) were diluted to 50 ng/uL. Samples were heated at 95 °C for 10 min and then put on ice immediately before loading on membranes. 50 ng, 100 ng, 150 ng or 200 ng DNA were loaded on Hybond N+ membranes (GE Healthcare Life Sciences). Membranes were air-dried and were crosslinked by UV stratalinker 2400 at 150

mJ/cm^2 twice. The membranes were then blocked for 1 hr in 5% milk in PBST (0.1% Tween-20), which were further subject to an overnight incubation with anti-6mA antibody (Synaptic Systems, 1: 1000) in 5% milk in PBST (0.1% Tween-20) at 4 °C. On the second day, membranes were washed 5 times for 5 min each with PBST (0.1% Tween-20) and then incubated with HRP-conjugated anti-rabbit IgG (Cell Signaling) for 1 hr at room temperature. Membranes were washed 5 times for 5 min each with PBST (0.1% Tween-20) before applied with ECL and developed.

RNA extraction and quantitative RT-PCR analyses—RNA expression level was tested by RT-qPCR. Total RNA was isolated by using RNeasy Plus Mini kit (Qiagen). 750 ng total RNA were reverse-transcribed into cDNA with PrimeScript™ RT reagent Kit (Takara), and then subjected to qPCR analysis with FastStart SYBR Green Master Mix (Roche) in a Roche LightCycler 96. *ACTB* and *B2M* were used as internal controls. Relative changes in expression were calculated using the $\Delta\Delta C_t$ method. All RT-qPCR primers are listed in Table S1.

mtDNA copy number quantification—mtDNA copy number was calculated based on the RT-qPCR method (Rooney et al., 2015) by using primers targeting mtDNA with genomic DNA as control (Table S1). Total DNA was extracted from cells by using PureLink Genomic DNA kit (Invitrogen) and was subjected to RT-qPCR analysis with FastStart SYBR Green Master Mix (Roche) in a Roche LightCycler 96.

siRNA knockdown and plasmid transfection—METTL4 siRNA was purchased (Qiagen SI04136671) with a target sequence AAGCCCTACGAAGGTATTATA. Transfection was achieved by using Lipofectamine RNAiMAX (Invitrogen) for siRNA or Lipofectamine 2000 (Invitrogen) for plasmids following the manufacturer's protocols. Knockdown efficiency was checked by using RT-qPCR or Western blot.

Lentivirus siRNA experiments—Lentivirus containing short hairpin RNAs (shRNAs) expressed in a lentiviral vector (pLKO.1-puro) were generated in HEK293T cells. The sequences and clonal names of plasmids are described in Key Resource Table. These plasmids and packaging plasmid pCMVΔR8.91 were provided by National RNAi Core Facility of Academia Sinica (Taipei, Taiwan). For lentivirus production, HEK293T cells were transfected with 5 μg lentiviral vectors expressing individual shRNA along with 0.5 μg of envelope plasmid pMD.G and 5 μg of packaging plasmid pCMVΔR8.91. Virus was collected 48 hr after transfection. To prepare METTL4 knockdown cells, cells were infected with lentivirus for 24 hr, and stable clones were generated by selection with appropriate antibiotics.

RNA-seq—Total RNA was isolated by using RNeasy Plus Mini kit (Qiagen) according to manufacturer protocol. mRNA was extracted from total RNA by using Dynabeads mRNA DIRECT kit (Ambion). For each sample, 50 ng of mRNA were used for library construction by using TruSeq stranded mRNA sample preparation kit (Illumina). Libraries were sequenced on Illumina Hiseq 4000.

6mA-ChIP-exo—6mA ChIP-exo 5.0 was performed according to the previous reported procedure (Rossi et al., 2018). Briefly, 1 μg mtDNA was sonicated to 200-400 bp and immunoprecipitated using anti-6mA antibody (Synaptic Systems, 202003 or NEB, E1610S) at 4 °C overnight. The antibody-DNA complex was then split into 96-well plate with 50 uL per well, irradiated by UV 254 nm with 0.15 mJ/cm^2 energy 5 times. The crosslinked samples were incubated with 80 μL pre-blocked Dynabeads Protein A (for SYSY) or Protein G (for NEB) slurry for 2 hr at 4 °C. A tailing, the first adapter ligation, kinase reaction, fill-in reaction and lambda exonuclease digestion were performed on beads. DNA was then released from beads and the purified DNA was subjected to splint ligation. The ligation product was amplified by PCR and libraries were subjected to high-throughput sequencing by using Illumina Nextseq500.

Quantification of 6mA in DNA and m^{6}A in RNA by UHPLC–QQQ–MS/MS— gDNA (150 ng) or mtDNA (50 ng) in 21.5 μL of nuclease-free H_2O was denatured at 95 °C for 10 min, then immediately chilled on ice for 2 min followed by digestion using 1 μL nuclease P1 (1 U/μL, Wako USA, 145-08221) in 10 mM NHÔAc (pH 5.3) at 42 °C overnight. On the next day, 3 μL 1 M NH_4HCO_3 solution and 1 μL of phosphodiesterase I from crotalus adamanteus venom (0.001 U, Sigma, P3243-1VL) were added. The mixture was incubated at 37 °C for 2 h and finally digested with 1 U FastAP Thermosensitive Alkaline Phosphatase and 3 μL 10× FastAP Buffer (Thermo Scientific, EF0651) at 37 °C for 4 hr. For RNA m^{6}A quantification, 50 ng RNA were digested by using 1 U nuclease P1 (Wako USA, 145-08221) in 20 μL reaction containing 20 mM NH_4OAc at 42 °C for 2 hr. Afterwards, 1 μL FastAP Thermosensitive Alkaline Phosphatase and 2.3 μL 10 × FastAP Buffer (Thermo Scientific, EF0651) was added and reaction was incubated at 37 °C for 2 hr. Digested DNA or RNA was diluted two folds with nuclease-free H2O and was filtered through 0.22 μm filter (Millipore, SLGVR04NL). For UHPLC‐QQQ–MS/MS analysis, 10 μL sample was injected and the nucleosides were separated by reverse-phase UHPLC on a C18 column (Agilent, 927,700-092) followed by MS detection using Agilent 6460 QQQ–MS/MS set to multiple reaction monitoring (MRM) in positive electrospray ionization mode. Nucleosides were quantified using the nucleoside precursor ion to base ion mass transitions of 266.1-150.0 for 6mA and 252.1-136.0 for dA. The concentration of nucleosides was quantified using the calibration curves which were obtained from nucleoside standards running at the same condition. The final ratio of 6mA/dA and m^{6}A/A were calculated by subtracting the background (mock control) derived from digestion enzymes.

***In vitro* DNA methylation assay—**150 ng ds-mtDNA or ss-mtDMA, 10 μM METTL4 protein and 0.8 mM d_3-SAM were mixed into 50 μL reaction buffer (80 mM KCl, 1.5 mM $MgCl_2$, 5 mM DTT, 4% glycerol and 15 mM HEPES pH 7.9). The reaction was performed at 16 °C for 14 hr. After incubation, the resultant DNA was purified by DNA Clean & Concentrator kit (Zymo Research) and was digested and quantified using method above.

Inner mitochondrial membrane potential (ΔΨm) detection—Inner mitochondrial membrane potential ΔΨm was measured following the protocol of TMRE (Jayaraman, 2005). Control cells and METTL4 knockdown cells were stained with 300 nM TMRE at 37 °C for 15 min. 20 μM carbonyl cyanide p-(trifluoromethoxy) phenylhydrazone (FCCP) was

added to cell culture media 10 minutes prior to staining with TMRE as a negative control. After TMRE staining, the culture medium was changed to PBS containing 0.2% BSA and kept on ice in the dark. Fluorescent signal of TMRE was immediately measured via Flow Cytometry LSR-Fortessa 4-15 HTS (BD digital instrument) with 10000 ungated cells acquired. TMRE is excited by the 561 nm yellow laser equipped in LSR-Fortessa and the emission around 610±20 nm was detected. Data was analyzed by FlowJo software version 10.0.8.

Mitochondria ROS detection—ROS production was measured using MitoTracker Red CM-H_2XROS (Molecular Probes), a widely used commercial probe for ROS detection in mitochondria. METTL4 knockdown cell and RNAi negative control cells were suspended in 1× HBSS buffer in 96-well white polystyrene microplates (Thermo). The time course of changes of fluorescence was recorded upon the addition of 2 μM MitoTracker Red CM-H2XROS using the Synergy HT (Bioteck, Winooski, VT) plate reader. CM-H2XROS MitoTracker was excited at 560±10 nm, and its emission was measured at 620±20 nm. The fluorescence intensity was calculated through averaging the results obtained from 8 samples (wells).

Cell proliferation assay—Cell proliferation assays were performed by seeding 3,000 cells in 96-well plate. METTL4 siRNA and Control siRNAs were transfected into cells using Lipofectamine RNAiMAX. The treated cells were incubated in 5% CO_2 at 37 °C for 24 hr, 48 hr or 72 hr after transfection. Cell viability was evaluated, at each experimental time point, by mixing with CellTiter 96 Aqueous One reagent (Promega) and incubating at 37 °C for 2 hr before reading absorbance. Intensity of absorbance was measured at an absorbance (A) wavelength of 490 nm using Synergy HT (Bioteck, Winooski, VT) plate reader. The signal was normalized to the value observed at 24 hr after seeding.

Cellular bioenergetics analysis using XFe96 extracellular flux analyzer—The influence of METTL4 on cell metabolic phenotype was measured using a Seahorse Bioscience XF96 analyzer (Seahorse Bioscience Inc.) and Seahorse XFp Cell Energy Phenotype Test Kit (Agilent) according to manufacturer's instructions. Briefly, both control and METTL4 knockdown cells were plated at a density of 2×10^4 cells per well with 4 replicates in Seahorse XF96 cell culture microplates (Agilent). Cells were grown overnight and incubated with XFp media for 1 hr in a non-CO_2 incubator before assay start. The 96-well sensor cartridge was hydrated in 200 μL water overnight then changed to XF calibrant solution (Seahorse Bioscience Inc.) for 1 hr incubation at 37 °C before plate calibration. For cell energy phenotype assay, cells were treated with 1 uM of oligomycin followed by three serial injections of FCCP in the final concentration of 0.5, 1 and 2 μM, respectively. For rho zero cells, 0.125, 0.25 and 0.5 μM FCCP was injected to cell subsequently. Seahorse Wave software (version 2.6) was used for data processing, including detection of outliers and cell number normalization. The final reports for the OCR and ECAR signals were generated using Seahorse XF Cell Energy Phenotype report generator.

Determination of specific mitochondrial electron transport chain complexes—50 μg of each protein sample was electrophoretically separated on a 4–15% gradient Mini-

Protean® TGX™ precast gel (Bio-Rad) at 60 V, transferred into a PVDF membrane (Bio-Rad). The blot was probed for 5 specific mitochondrial electron transport chain complexes using a human total OXPHOS cocktail (Abcam, ab110411) which includes five monoclonal antibodies specific for complex I subunit NDUFB8, complex II subunit SDHB, complex III subunit UQCRC2, complex IV subunit COX II, and complex V subunit ATP5A. Antibody against β-actin was used as an internal control.

***In vitro* transcription—**Purified recombinant POLRMT (134 kDa), human TFAM (26.6 kDa, aa 43–246) and TFB2M (45.8 kDa, aa 20–396) are purchased from Enzymax. Excess DNA Fragment 1 (Table S4) harboring with or without one 6mA at the HSP and LSP promoter were ligated with fragment 2 of HSP and LSP (Table S4) using T4 DNA ligase. The ligated products were purified twice using AMPure XP beads (Beckman Coulter) according to the protocol for size selection to remove the excess short fragment 1 and unannealed ssDNA. The transcription reactions were performed in a total volume of 10 μL. 2 μL 50 nM DNA templates were mixed with 2 μL 5× transcription buffer (50 mM HEPES pH 7.7, 500 mM NaCl, 50 mM $MgCl_2$, 5 mM DTT, 0.5 μg/μL BSA), followed by incubating at 32 °C for 5 min. 1 μL 2 μM TFAM was then added and the mixtures were incubated at room temperature for 1 min. 1 μL 500 nM TFB2M was then added and the mixtures were incubated at room temperature for another 1 min. 1 μL 500 nM POLRMT was then added and the reaction mixtures were incubated at 32 °C for 5 min. Finally, 2.5 μL 4× NTP mix (2 mM ATP, 2 mM GTP, 2 mM CTP, 40 μM UTP, supplemented with 0.8 μCi/μL [α-^{32}P] UTP) and 0.5 μL SUPERNase Inhibitor (Invitrogen) were added to initiate the reactions. Reactions were carried out at 32 °C for 45 min and were cleaned-up by RNA Clean and Concentrator (Zymo). The run-off products were resolved by using 6% Novex TBE-Urea gel at 120 V for 1 hr and visualized by phosphor imaging (Amersham Typhoon 5 Biomolecular Imager). The quantification of transcripts was performed using ImageJ software using the results of two independent experiments.

Immunoelectron microscopy—Cells and tissues were fixed with 4% paraformaldehyde with 0.15% glutaraldehyde in 0.1M PB buffer for 1 h. After fixation, cells and tissues were washed 3 times with 0.1 M PB buffer for 20 min each. Dehydration was performed in the following sequence: 30% ethanol for 15 min; 50% ethanol for 15 min; 70% ethanol for 15 min; 95% ethanol for 15 min; 100% ethanol for 15 min. Infiltration was performed in a 1:1 mixture of 100% ethanol: L.R. White (medium grade) with gentle agitation for 1 hr at room temperature followed by overnight infiltration with fresh L.R. White medium. On the next day, change fresh L.R. white medium 4-6 times. For embedding step: cells or tissues were filled in gelatin capsules with resin and polymerized in vacuum oven at 45 °C for 48 hr. 80 nm thickness sections were cut by Reichert-Jung Ultracut E. and mount on formvar/carbon coated 200 mesh gold grids. For immunogold labeling, grids were rehydrated with PBS for 30 min at room temperature, blocked with 1% BSA in PBS for 30 min. Grids were then transferred into 1:10 diluted METTL4 antibody (HPA040061, Sigma) in 1% BSA, incubated at humidified chamber for 3.5 hr at room temperature. After incubation, grids were washed 6 times with PBS for 10 min each and further blocked with 0.5% BSA in PBS for 25 min. The secondary antibody (10 nm gold-conjugated EM, TED PELLA, INC) was diluted 1:10 in 0.5% BSA and incubated with blocked grids for 1 hour at room temperature. Grids were

washed with PBS 3 times and was fixed with 1% glutaraldehyde in PBS for 10 min followed by washing with aqua 3 times with 5 min each and stained briefly with uranyl acetate and lead citrate. Air dry the grids and then examine the grids under 300 KV at FEI Tecnai F30.

Evaluation the level of nascent mitochondrial polycistronic precursor RNA—5-ethynyl uridine (5-EU) labeling of nascent RNA was performed using the Click-iT® Nascent RNA Capture Kit (Life Technologies) following the manufacture's instruction. In brief, control and METTL4 knockdown HepG2 cells were treated with 5'-ethynyl-uridine (5-EU) at the final concentration of 0.5 mM, and cells were harvest after 10, 20, 30- and 60-min treatment. Total RNA was extracted using TRIzol reagent (Cat. No. 155596-018). 750 ng 5-EU-RNA was used for biotinylation by Click reaction using the Click-iT® Nascent RNA Capture Kit (Life Technologies) protocol. After RNA precipitation and purification, 250 ng of biotinylated RNA was used for pull-down with 15 μL Dynabeads® MyOne™ Streptavidin T1 magnetic beads. Biotinylated RNA bound to beads was serially washed, and the bound RNA was reverse transcribed using the Recombinant HIV Reverse Transcriptase (Worthington Biochemiclal Corporation). RT-qPCR analysis was performed using primers (Table S1) that span the splice junctions of pre-mtRNA to ensure that only transcribed polycistronic pre-RNAs can be amplified. All RT-qPCRs were performed using the method shown above with two biological replicates and 2 technical replicates.

***In vitro* pull-down assay—**6mA modified and unmodified HSP or LSP probes were mixed at 1:1 ratio to the final concentration of 1 μM in TFAM binding buffer (50 mM KCl, 5 mM $MgCl_2$, 10% glycerol and 10 mM Tris-HCl, pH 7.8). Save 1/3 from the same sample as input, TFAM was then added into the DNA mixture at the final concentration of 10 μM in 20 μL reaction system and incubated at room temperature 20 min. 20 μL His-affinity magnetic beads (Dynabeads His-Tag isolation and pulldown, Invitrogen) were used for each sample after being washed four times with 200 μL IPP buffer for each wash. The beads were then re-suspended in 180 μL IPP buffer and incubated with TFAM–DNA mixture for another 1 hr with rotation at 4 °C. The aqueous phase was collected, recovered by ethanol precipitation, dissolved in 20 μL water, and saved as the flow-through. The beads were washed four times with 300 μL 1× IPP buffer each time. TFAM–DNA complex was eluted twice with 300 mM imidazole in 100 μL IPP buffer. 30 μg Proteinase K was added to digest DNA bounded TFAM and the DNA was further recovered by ethanol precipitation. The purified fraction was dissolved in 20 μL water, saved as TFAM-bounded. LC-MS/MS was used to measure the level of m^6A in each sample of input, flow-through and TFAM-bound.

EMSA assay—DNA probes containing TFAM binding sites with or without 6mA was used for this assay. All EMSA reaction mixtures in this study were set up in a final volume of 20 μL containing 20 nM annealed double-stranded DNA (Table S4), increased concentration of TFAM (10 nM to 60 nM for LSP and 20 to 120 nM for HSP) in binding buffer (50 mM KCl, 5 mM $MgCl_2$, 10% glycerol and 10 mM Tris-HCl, pH 7.8). The binding reaction was performed at room temperature for 10 min. Samples were loaded onto the 4-12% TBE gel (Thermo Fisher) and were run in 0.5× TB buffer (tenfold dilution from 5× TB buffer: 50 mM Tris-HCl, 41.5 mM borate, pH 7.8) at 110 V for 1 hr at 4 °C. Gels were

stained in a 10,000-fold diluted SYBR Gold nucleic acid staining solution for 7 min. The DNA bands were visualized with UV light at 254 nm.

FRET assay for DNA bending—FRET probes (Table S4) with or without 6mA modification were annealed according to a previous protocol (Ngo et al., 2013). DNA probes include Cy3-Cy5 double-labeled DNA containing both donor and acceptor fluorophores, Cy3-labeled DNA containing only the donor fluorophore, and Cy5-only DNA that contains only the acceptor fluorophore. The annealed DNAs with singly labeled Cy3 or Cy5 fluorophore, respectively, were included to obtain correction factors for FRET efficiency calculation. The FRET measurements were recorded on a FluoroMax-3 spectrofluorimeter (Jobin–Yvon–Horiba) at room temperature. 200 nM TFAM protein was added into a cuvette containing either 40 nM 6mA modified or unmodified FRET probes (Cy3-labeled, Cy5-labeled or Cy3-Cy5-labeled DNA) in binding buffer (20vmM Tris-HCl pH 7.5, 150 mM NaCl, 1 mM DTT). Raw FRET was observed by using excitation at 525 nm and measuring emission from 640 to 750 nm (FRET signal). Two correction measurements were made as follows: excitation wavelength for Cy3-only DNA was excited at 525 nm and the emission measured from 550 to 580 nm (Donor signal). Excitation wavelength for Cy5-labeled DNA was excited at 625 nm and emission from 640 to 750 nm were recorded (Acceptor signal). Slit widths for excitation and emission were 4 nm and 10 nm, respectively. The FRET efficiency (E) was calculated with the following formula:

$$E = (F_{corr}) / (F_{corr} + D_{corr})$$

Fcorr and Dcorr are the corrected FRET and donor florescence, respectively.

$$F_{corr} = [F-(\chi_D)\cdot(\chi_A)] / \sigma_A,\ D_{corr} = D_{\sigma D}$$

The correction factor for donor bleed-through (χ_D) was determined using the Cy3-only DNA in the absence of TFAM. χ_D = (F/D), where F and D are the raw FRET signal and donner fluorescence of Cy3-only DNA, respectively. The correction factor for direct excitation of the acceptor (χ_A) was determined using the Cy5-only DNA in the absence of TFAM. χ_A =(F/A), the raw FRET signal (F) was divided by the acceptor signal (A). Next, to account for changes in fluorescence emission caused by FRET-independent TFAM interaction, two additional correction factors were determined: σ_D was calculated using the data obtained with the Cy3-only DNA and dividing the donor signal of TFAM-bound DNA by unbound DNA, $\sigma D = D_b/D_u$. σ_A was calculated using the data obtained with the Cy5-only DNA and dividing the acceptor signal of TFAM-bound DNA by unbound DNA, $\sigma A = A_b/A_u$.

QUANTIFICATION AND STATISTICAL ANALYSIS

RNA-seq data analysis—For RNA-seq, about 33 million raw single-end reads were obtained for each biological replicate. Reads were first trimmed for adaptor sequences and low-quality nucleotides, and then aligned to human hg19 reference genome and transcriptome using Hisat software (Li et al., 2015). Reads mapped to multiple loci in the

genome or mapped to tRNA/rRNA regions were excluded for further downstream analysis (Table S2). RPKM values for all samples were generated by Cuffnorm software using geometric library normalization method. Expression heatmaps were visualized using pheatmap R package with z-scores calculated for each row. For splicing analysis, reads were mapped to human genome and transcriptome (hg38, version 29, 2018-08-30) with TopHat v2.1.1. Splicing evens were estimated with rMATS (version 4.0.2), and those events with average junction (inclusion junction and skipping junction) reads <= 10 in either group were filtered out. Significant deferentially spliced events were identified as events with |delta PSI| (METTL4 KO vs. Control) more than 0.05 and FDR < 0.05.

6mA ChIP-exo data analysis—Illumina sequencing reads were first trimmed to discard adapter sequences and low-quality nucleotides, then mapped to hg19 reference genome using Bowtie. To avoid NUMTs-induced false positives, we performed unique mapping in 6mA ChIP-exo analysis. Only uniquely mapped reads that exclusively mapped to mitochondria DNA, but not nuclear DNA were further kept for downstream analysis (Table S3). Normalized BigWig files were generated based on reads aligned to chrM only. For peak calling, reads were counted on consecutive 10-bp windows of mitochondria DNA by FeatureCounts. Normalization was conducted using DESeq2. As mitochondrial genome is small (enrichment background is high), a cutoff with log2(fold change) > 0.1 and normalized reads larger than 30 were used to call peaks. Circos map was used for tracks visualization.

DATA AND SOFTWARE AVAILABILITY

Raw and analyzed data for all sequencing experiments have been deposited at the GEO (https://www.ncbi.nlm.nih.gov/geo/) under accession number GSE102670. Imaging data have been deposited to Mendeley data (DOI: 10.17632/6byrgvmc59.1).

Supplementary Material

Refer to Web version on PubMed Central for supplementary material.

ACKNOWLEDGMENTS

We thank Yau-Huei Wei for the rho zero cells, and Jun Liu, Hsin-Chen Lee and Guanzheng Luo for suggestions. We are greatful to Dr. Qin Jin, Dr. Pieter W. Faber and Dr. Yimei Chen for assisting experiments. We would like to thank Life Science Editors for editorial assistance. L.H. is a Leukemia & Lymphoma Society's Career Development Special Fellow. C.H. is supported by NIH (HG008935, NS097206, and HG006827). K.J.W is supported by Ministry of Science and Technology (Taiwan) Summit grant (MOST 106-2745-B-039-001). C. H. is an Investigator of the Howard Hughes Medical Institute.

REFERENCES

Agaronyan K, Morozov YI, Anikin M, and Temiakov D (2015). Replication-transcription switch in human mitochondria. Science 347, 548–551. [PubMed: 25635099]

Alam TI, Kanki T, Muta T, Ukaji K, Abe Y, Nakayama H, Takio K, Hamasaki N, and Kang D (2003). Human mitochondrial DNA is packaged with TFAM. Nucleic acids Res 31, 1640–1645. [PubMed: 12626705]

Bang J, Bae S-H, Park C-J, Lee J-H, and Choi B-S (2008). Structural and dynamics study of DNA dodecamer duplexes that contain un-, hemi-, or fully methylated GATC sites. J Am Chem Soc 130, 17688–17696. [PubMed: 19108701]

Baubec T, and Schubeler D (2014). Genomic patterns and context specific interpretation of DNA methylation. Curr Opin Genet Dev 25, 85–92. [PubMed: 24614011]

Beh LY, Debelouchina GT, Clay DM, Thompson RE, Lindblad KA, Hutton ER, Bracht JR, Sebra RP, Muir TW, and Landweber LF (2019). Identification of a DNA N6-Adenine Methyltransferase Complex and Its Impact on Chromatin Organization. Cell 177, 1781–1796.e1725. [PubMed: 31104845]

Bestwick ML, and Shadel GS (2013). Accessorizing the human mitochondrial transcription machinery. Trends Biochem Sci 38, 283–291. [PubMed: 23632312]

Bird A (2007). Perceptions of epigenetics. Nature 447, 396. [PubMed: 17522671]

Bleier L, and Dröse S (2013). Superoxide generation by complex III: From mechanistic rationales to functional consequences. BBA-Bioenergetics 1827, 1320–1331. [PubMed: 23269318]

Bonawitz ND, Clayton DA, and Shadel GS (2006). Initiation and beyond: multiple functions of the human mitochondrial transcription machinery. Mol Cell 24, 813–825. [PubMed: 17189185]

Campbell CT, Kolesar JE, and Kaufman BA (2012). Mitochondrial transcription factor A regulates mitochondrial transcription initiation, DNA packaging, and genome copy number. BBA-Gene Regul Mech 1819, 921–929.

Chen H, Gu L, Orellana EA, Wang Y, Guo J, Liu Q, Wang L, Shen Z, Wu H, Gregory RI, et al. (2020). METTL4 is an snRNA m6Am methyltransferase that regulates RNA splicing. Cell Res.

Chen Q, Vazquez EJ, Moghaddas S, Hoppel CL, and Lesnefsky EJ (2003). Production of Reactive Oxygen Species by Mitochondria: CENTRAL ROLE OF COMPLEX III. J Biol Chem 278, 36027–36031. [PubMed: 12840017]

Chen Z-X, and Riggs AD (2011). DNA methylation and demethylation in mammals. J Biol Chem 286, 18347–18353. [PubMed: 21454628]

Degli Esposti M (2002). Measuring mitochondrial reactive oxygen species. Methods 26, 335–340. [PubMed: 12054924]

Ehrlich M, and Wang R (1981). 5-Methylcytosine in eukaryotic DNA. Science 212, 1350–1357. [PubMed: 6262918]

Farge G, Mehmedovic M, Baclayon M, van den Wildenberg, Siet MJL, Roos Wouter H., Gustafsson Claes M., Wuite Gijs J.L., and Falkenberg M (2014). *In vitro*-reconstituted nucleoids can block mitochondrial DNA replication and transcription. Cell Rep 8, 66–74. [PubMed: 24981867]

Fazakerley GV, Gabarro-Arpa J, Lebret M, Guy A, and Guschlbauer W (1989). The GTm6AC sequence is overwound and bent. Nucleic Acids Res 17, 2541–2556. [PubMed: 2717401]

Fu Y, Luo G-Z, Chen K, Deng X, Yu M, Han D, Hao Z, Liu J, Lu X, Dore Louis C., et al. (2015). N6-Methyldeoxyadenosine marks active transcription start sites in *Chlamydomonas*. Cell 161, 879–892. [PubMed: 25936837]

Fuhrmann DC, and Brune B (2017). Mitochondrial composition and function under the control of hypoxia. Redox Biol 12, 208–215. [PubMed: 28259101]

Gould MP, Bosworth CM, McMahon S, Grandhi S, Grimerg BT, and LaFramboise T (2015). PCR-Free Enrichment of Mitochondrial DNA from Human Blood and Cell Lines for High Quality Next-Generation DNA Sequencing. PLOS ONE 10, e0139253. [PubMed: 26488301]

Gray MW (2012). Mitochondrial evolution. Cold Spring Harb Perspec Biol 4 a011403

Greer Eric L., Blanco Mario A., Gu L, Sendinc E, Liu J, Aristizabal-Corrales D, Hsu C-H, Aravind L, He C, and Shi Y (2015). DNA Methylation on N6-Adenine in *C. elegans*. Cell 161, 868–878. [PubMed: 25936839]

Guzy RD, Hoyos B, Robin E, Chen H, Liu L, Mansfield KD, Simon MC, Hammerling U, and Schumacker PT (2005). Mitochondrial complex III is required for hypoxia-induced ROS production and cellular oxygen sensing. Cell Metab 1, 401–408. [PubMed: 16054089]

Hatefi Y (1985). The mitochondrial electron transport and oxidative phosphorylation system. Annu Rev Biochem 54, 1015–1069. [PubMed: 2862839]

Iyer LM, Zhang D, and Aravind L (2016). Adenine methylation in eukaryotes: Apprehending the complex evolutionary history and functional potential of an epigenetic modification. BioEssays 38, 27–40. [PubMed: 26660621]

Jayaraman S, (2005) Flow cytometric determination of mitochondrial membrane potential changes during apoptosis of T lymphocytic and pancreatic beta cell lines: Comparison of tetramethylrhodamineethylester (TMRE), chloromethyl-X-rosamine (H2-CMX-Ros) and MitoTracker Red 580 (MTR580). J. Immunol. Methods 306, 68–79. [PubMed: 16256133]

Jones PA, and Takai D (2001). The role of DNA methylation in mammalian epigenetics. Science 293, 1068–1070. [PubMed: 11498573]

Kim D, Langmead B, Salzberg SL, (2015) HISAT: a fast spliced aligner with low memory requirements. Nature Methods 12, 357–360. [PubMed: 25751142]

King M, and Attardi G (1989). Human cells lacking mtDNA: repopulation with exogenous mitochondria by complementation. Science 246, 500–503. [PubMed: 2814477]

Koziol MJ, Bradshaw CR, Allen GE, Costa ASH, Frezza C, and Gurdon JB (2016). Identification of methylated deoxyadenosines in vertebrates reveals diversity in DNA modifications. Nat Struct Mol Biol 23, 24–30. [PubMed: 26689968]

Kukat C, Davies KM, Wurm CA, Spahr H, Bonekamp NA, Kühl I, Joos F, Polosa PL, Park CB, Posse V, et al. (2015). Cross-strand binding of TFAM to a single mtDNA molecule forms the mitochondrial nucleoid. Proc Natl Acad Sci USA 112, 11288–11293. [PubMed: 26305956]

Lezza AMS (2012). Mitochondrial transcription factor A (TFAM): one actor for different roles. Front Biol 7, 30–39.

Li M, Zhong Z, Zhu J, Xiang D, Dai N, Cao X, Qing Y, Yang Z, Xie J, Li Z, et al. (2010). Identification and characterization of mitochondrial targeting sequence of human apurinic/apyrimidinic endonuclease 1. J Biol Chem. 285, 14871–14181 [PubMed: 20231292]

Liu J, Yue Y, Han D, Wang X, Fu Y, Zhang L, Jia G, Yu M, Lu Z, Deng X, et al. (2014). A METTL3-METTL14 complex mediates mammalian nuclear RNA N6-adenosine methylation. Nat Chem Biol 10, 93–95. [PubMed: 24316715]

Liu J, Zhu Y, Luo G-Z, Wang X, Yue Y, Wang X, Zong X, Chen K, Yin H, Fu Y, et al. (2016). Abundant DNA 6mA methylation during early embryogenesis of zebrafish and pig. Nat Comm 7, 13052.

Lluch-Senar M, Luong K, Lloréns-Rico V, Delgado J, Fang G, Spittle K, Clark TA, Schadt E, Turner SW, Korlach J, et al. (2013). Comprehensive methylome characterization of *Mycoplasma genitalium* and *Mycoplasma pneumoniae* at single-base resolution. PLoS Genet 9, e1003191. [PubMed: 23300489]

Luo G-Z, Blanco MA, Greer EL, He C, and Shi Y (2015). DNA N6-methyladenine: a new epigenetic mark in eukaryotes? Nat Rev Mol Cell Biol 16, 705. [PubMed: 26507168]

Luo G-Z, Hao Z, Luo L, Shen M, Sparvoli D, Zheng Y, Zhang Z, Weng X, Chen K, Cui Q, et al. (2018). N6-methyldeoxyadenosine directs nucleosome positioning in Tetrahymena DNA. Genome Biol 19, 200. [PubMed: 30454035]

Luo GZ, and He C (2017). DNA N6-methyladenine in metazoans: functional epigenetic mark or bystander? Nat Struct Mol Biol 24, 503–506. [PubMed: 28586322]

Ma C, Niu R, Huang T, Shao L-W, Peng Y, Ding W, Wang Y, Jia G, He C, Li C-Y, et al. (2019). N6-methyldeoxyadenine is a transgenerational epigenetic signal for mitochondrial stress adaptation. Nat Cell Biol 21, 319–327. [PubMed: 30510156]

Maunakea AK, Nagarajan RP, Bilenky M, Ballinger TJ, D'Souza C, Fouse SD, Johnson BE, Hong C, Nielsen C, Zhao Y, et al. (2010). Conserved role of intragenic DNA methylation in regulating alternative promoters. Nature 466, 253. [PubMed: 20613842]

Mercer Tim R., Neph S, Dinger Marcel E., Crawford J, Smith Martin A., Shearwood A.- Marie J., Haugen E, Bracken Cameron P., Rackham O, Stamatoyannopoulos John A., et al. (2011). The human mitochondrial transcriptome. Cell 146, 645–658. [PubMed: 21854988]

Mondo SJ, Dannebaum RO, Kuo RC, Louie KB, Bewick AJ, LaButti K, Haridas S, Kuo A, Salamov A, Ahrendt SR, et al. (2017). Widespread adenine N6-methylation of active genes in fungi. Nat Genet 49, 964. [PubMed: 28481340]

Murphy Michael P. (2009). How mitochondria produce reactive oxygen species. Biochem J 417, 1–13. [PubMed: 19061483]

Ngo HB, Kaiser JT, and Chan DC (2011). The mitochondrial transcription and packaging factor Tfam imposes a U-turn on mitochondrial DNA. Nat Struct Mol Biol 18, 1290–1296. [PubMed: 22037171]

Ngo HB, Lovely GA, Phillips R, Chan DC (2014) Distinct structural features of TFAM drive mitochondrial DNA packaging versus transcriptional activation. Nat. Commun 5, 3077–3088. [PubMed: 24435062]

Pfanner N, and Geissler A (2001). Versatility of the mitochondrial protein import machinery. Nat Rev Mol Cell Biol 2, 339. [PubMed: 11331908]

Polaczek P, Kwan K, and Campbell JL (1998). GATC motifs may alter the conformation of DNA depending on sequence context and N6-adenine methylation status: possible implications for DNA-protein recognition. Mol Gen Genet 258, 488–493. [PubMed: 9669330]

Quispe-Tintaya W, White RR, Popov VN, Vijg J, and Maslov AY (2013). Fast mitochondrial DNA isolation from mammalian cells for next-generation sequencing. BioTechniques 55, 133–136. [PubMed: 24003945]

Reinecke F, Smeitink JAM, and van der Westhuizen FH (2009). OXPHOS gene expression and control in mitochondrial disorders. BBA-Mol Basis Dis 1792, 1113–1121.

Rooney JP, Ryde IT, Sanders LH, Howlett EH, Colton MD, Germ KE, Mayer GD, Greenamyre JT, Meyer JN (2015) PCR Based Determination of Mitochondrial DNA Copy Number in Multiple Species. Methods Molecular Biology 1241, 23–38.

Rossi MJ, Lai WKM, and Pugh BF (2018). Simplified ChIP-exo assays. Nat Commun 9, 2842. [PubMed: 30030442]

Roundtree IA, Evans ME, Pan T, and He C (2017). Dynamic RNA modifications in gene expression regulation. Cell 169, 1187–1200. [PubMed: 28622506]

Saraste M (1999). Oxidative Phosphorylation at the fin de siecle. Science 283, 1488–1493. [PubMed: 10066163]

Schiffers S, Ebert C, Rahimoff R, Kosmatchev O, Steinbacher J, Bohne A-V, Spada F, Michalakis S, Nickelsen J, Muller M, et al. (2017). Quantitative LC-MS provides no evidence for m6dA or m4dC in the genome of mouse embryonic stem cells and tissues. Angew Chem Int Ed 56, 1268–11271.

Semenza GL (2012). Hypoxia-inducible factors: mediators of cancer progression and targets for cancer therapy. Trends Pharmacol Sci 33, 207–214. [PubMed: 22398146]

Smith AC, and Robinson AJ (2018). MitoMiner v4.0: an updated database of mitochondrial localization evidence, phenotypes and diseases. Nucleic Acids Res 47, D1225–D1228.

Uchida A, Murugesapillai D, Kastner M, Wang Y, Lodeiro MF, Prabhakar S, Oliver GV, Arnold JJ, Maher LJ III, Williams MC, et al. (2017). Unexpected sequences and structures of mtDNA required for efficient transcription from the first heavy-strand promoter. eLife 6, e27283. [PubMed: 28745586]

Van der Wijst MGP, and Rots MG (2015). Mitochondrial epigenetics: an overlooked layer of regulation? Trends Genet 31, 353–356. [PubMed: 25891224]

Wang P, Doxtader Katelyn A., and Nam Y (2016a). Structural basis for cooperative function of Mettl3 and Mettl14 methyltransferases. Mol Cell 63, 306–317. [PubMed: 27373337]

Wang W, Xu L, Hu L, Chong J, He C, and Wang D (2017). Epigenetic DNA modification N6-Methyladenine causes site-specific RNA polymerase II transcriptional pausing. J Am Chem Soc 139, 14436–14442. [PubMed: 28933854]

Wang X, Feng J, Xue Y, Guan Z, Zhang D, Liu Z, Gong Z, Wang Q, Huang J, Tang C, et al. (2016b). Structural basis of N6-adenosine methylation by the METTL3–METTL14 complex. Nature 534, 575. [PubMed: 27281194]

Wang Y, Li Y, Toth JI, Petroski MD, Zhang Z, and Zhao JC (2014). N6-methyladenosine modification destabilizes developmental regulators in embryonic stem cells. Nature Cell Biol 16, 191. [PubMed: 24394384]

Weber M, Hellmann I, Stadler MB, Ramos L, Pääbo S, Rebhan M, and Schübeler D (2007). Distribution, silencing potential and evolutionary impact of promoter DNA methylation in the human genome. Nature Genet 39, 457. [PubMed: 17334365]

Wiedemann N, Frazier AE, and Pfanner N (2004). The Protein Import Machinery of Mitochondria. J Biol Chem 279, 14473–14476. [PubMed: 14973134]

Wion D, and Casadesus J (2006). N6-methyl-adenine: an epigenetic signal for DNA-protein interactions. Nat Rev Micro 4, 183–192.

Wright R, Stephens C, and Shapiro L (1997). The CcrM DNA methyltransferase is widespread in the alpha subdivision of proteobacteria, and its essential functions are conserved in Rhizobium meliloti and Caulobacter crescentus. J Bacteriol 179, 5869–5877. [PubMed: 9294447]

Wu H, and Zhang Y (2013). Reversing DNA Methylation: Mechanisms, Genomics, and Biological Functions. Cell 156, 45–68.

Wu TP, Wang T, Seetin MG, Lai Y, Zhu S, Lin K, Liu Y, Byrum SD, Mackintosh SG, Zhong M, et al. (2016). DNA methylation on N6-adenine in mammalian embryonic stem cells. Nature 532, 329–333. [PubMed: 27027282]

Xie Q, Wu TP, Gimple RC, Li Z, Prager BC, Wu Q, Yu Y, Wang P, Wang Y, Gorkin DU, et al. (2018). N6-methyladenine DNA Modification in Glioblastoma. Cell 175, 1228–1243.e1220. [PubMed: 30392959]

Yao B, Cheng Y, Wang Z, Li Y, Chen L, Huang L, Zhang W, Chen D, Wu H, Tang B, et al. (2017). DNA N6-methyladenine is dynamically regulated in the mouse brain following environmental stress. Nat Comm 8, 1122.

Zhang G, Huang H, Liu D, Cheng Y, Liu X, Zhang W, Yin R, Zhang D, Zhang P, Liu J, et al. (2015). N6-methyladenine DNA modification in Drosophila. Cell 161, 893–906. [PubMed: 25936838]

Zhang X, Yazaki J, Sundaresan A, Cokus S, Chan SWL, Chen H, Henderson IR, Shinn P, Pellegrini M, Jacobsen SE, et al. (2006). Genome-wide high-resolution mapping and functional analysis of DNA methylation in *Arabidopsis*. Cell 126, 1189–1201. [PubMed: 16949657]

HIGHLIGHTS

- *N*-methyldeoxyadenosine (6mA) is enriched in human mitochondria DNA (mtDNA)
- METTL4 can mediate mammalian mtDNA 6mA methylation
- mtDNA 6mA affects mitochondrial transcription, replication, and activity
- The 6mA level in mtDNA is significantly elevated under hypoxic stress

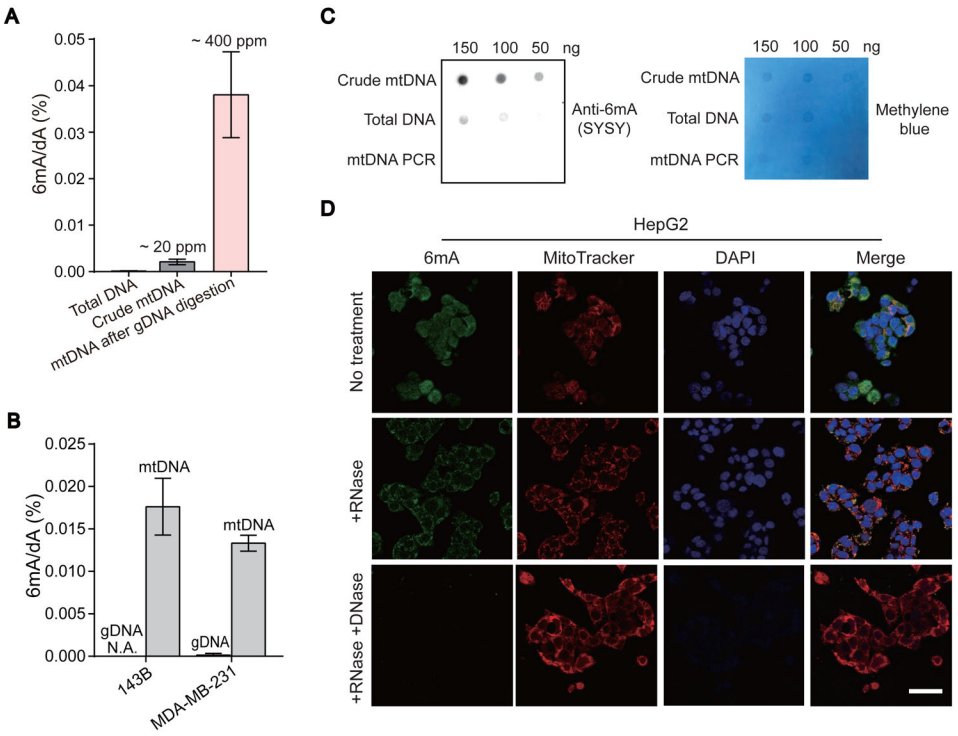

Figure 1. The Presence of N^6-deoxyadenosine Methylation (6mA) in Human Mitochondrial DNA (mtDNA)

(A) UHPLC-QQQ-MS/MS showing 6mA/dA levels in total DNA, crude mtDNA, and DNase digested mtDNA in HepG2 cells (n = 3, mean ± SEM).

(B) UHPLC-QQQ-MS/MS showing 6mA levels in gDNA and mtDNA in 143B cells and MDA-MB-231 cells (n = 2, mean ± SEM).

(C) 6mA dot blot of total DNA, crude mtDNA, and PCR amplified mtDNA.

(D) 6mA signals (green) and their co-localization with mitochondria marker (red) in HepG2 cells with no treatment, RNase treatment, and DNase + RNase treatment; scale bar: 100 μm. See also Figure S1 and S2.

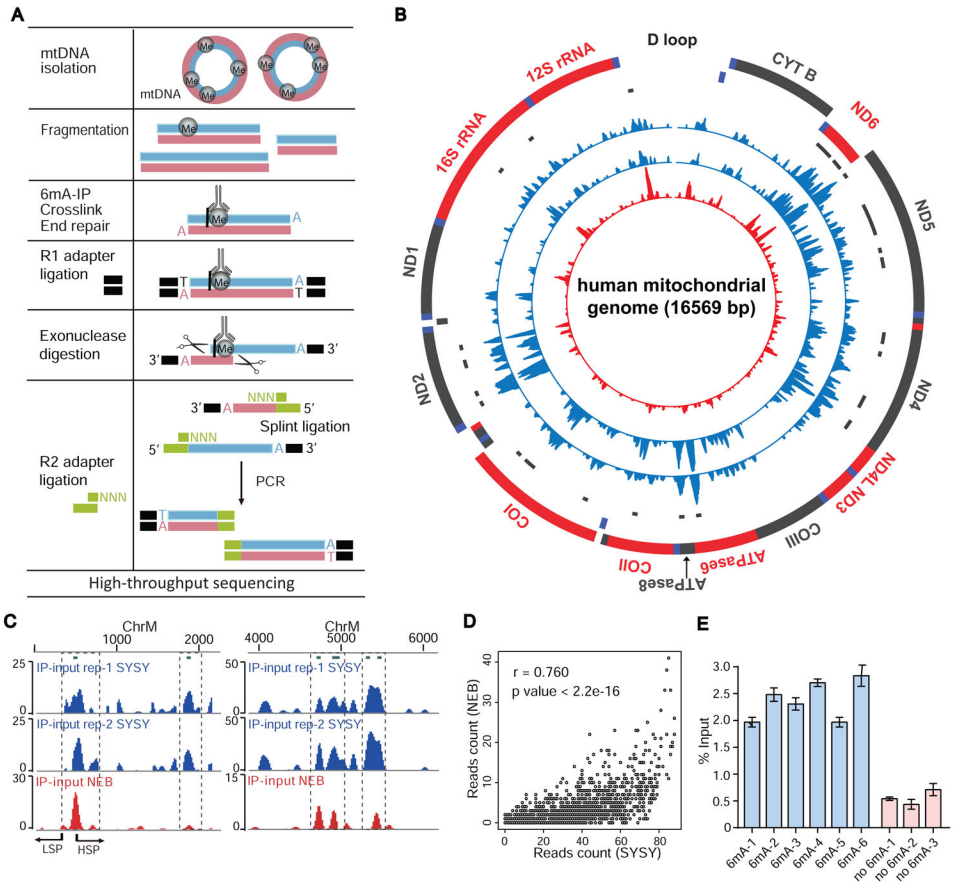

Figure 2. The Distribution of 6mA in Human mtDNA

(A) The workflow of 6mA ChIP-exo.

(B) Circos plot of 6mA distributions in mtDNA. Mitochondrial genome is shown as the outermost circle in red/gray/blue with gene annotations. 6mA profiles (IP - input) revealed by SYSY-IP rep-1 (blue), SYSY-IP rep-2 (blue), and NEB-IP (red) were show in three tracks, respectively, from outside to inside. Gray dots and bars indicate 6mA peaks. Reads from input libraries have been subtracted.

(C) Two zoomed in regions from (B), showing examples of 6mA peaks (IP - input) detected by both SYSY and NEB antibodies. Reads from input libraries have been subtracted. The left penal showed the peak detected on the promotor region.

(D) Spearman correlation analysis of 6mA-IP profiles generated from using NEB and SYSY anti-6mA antibodies, respectively. Spearman r = 0.760.

(E) 6mA-IP qPCR validation of 6mA-posotive and 6mA-negative sites revealed by 6mA mapping (n = 2, mean ± SEM).

See also Figure S2.

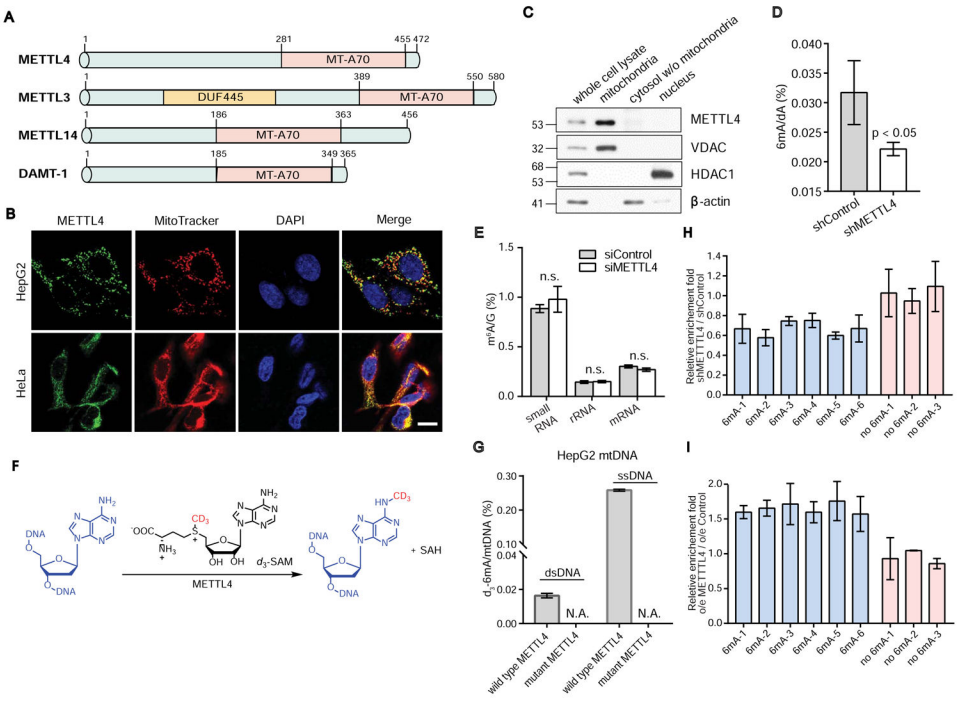

Figure 3. METTL4 is Enriched in Mitochondrion and Mediates mtDNA 6mA Methylation

(A) Multiple alignments of METTL4 to METTL3/METTL14 and DAMT-1.

(B) Immunofluorescence displayed the co-localization of METTL4 with mitochondria in HepG2 and HeLa cells. Scale bar: 20 μm. The co-localization of METTL4 with mitochondria was evaluated by Pearson correlation coefficient, with Rr = 0.60 for HepG2 and 0.74 for HeLa.

(C) Western blot revealed the uneven distribution of the METTL4 protein in different subcellular fractions and the enrichment of METTL4 in mitochondria. VDAC (mitochondrial), β-actin (cytosolic), and HDAC1 (nuclear) were chose as compartment-specific markers demonstrating the purity of each subcellular fraction.

(D) Knockdown of METTL4 resulted in a decrease of the total 6mA level in HepG2 mtDNA ($n = 4$, $p < 0.05$, t test, mean ± SEM).

(E) Knockdown METTL4 did not reduce the m^6A level in mtRNA species ($n = 4$, mean ± SEM).

(F) Schematic illustration of *N*-deoxyadenosine methylation of DNA in the presence of METTL4 and d_3-SAM.

(G) The *in vitro* methylation activity of METTL4 and its inactive mutant on single-stranded and double-stranded mtDNA ($n = 2$, mean ± SEM).

(H) 6mA-IP qPCR of 6mA-positive and 6mA-negative sites revealed by 6mA mapping in stable METTL4 knockdown HepG2 and control cells ($n = 2$, mean ± SEM).

(I) 6mA-IP qPCR of 6mA-positive and 6mA-negative sites revealed by 6mA mapping in METTL4 overexpression and control cells ($n = 2$, mean ± SEM).

See also Figure S3.

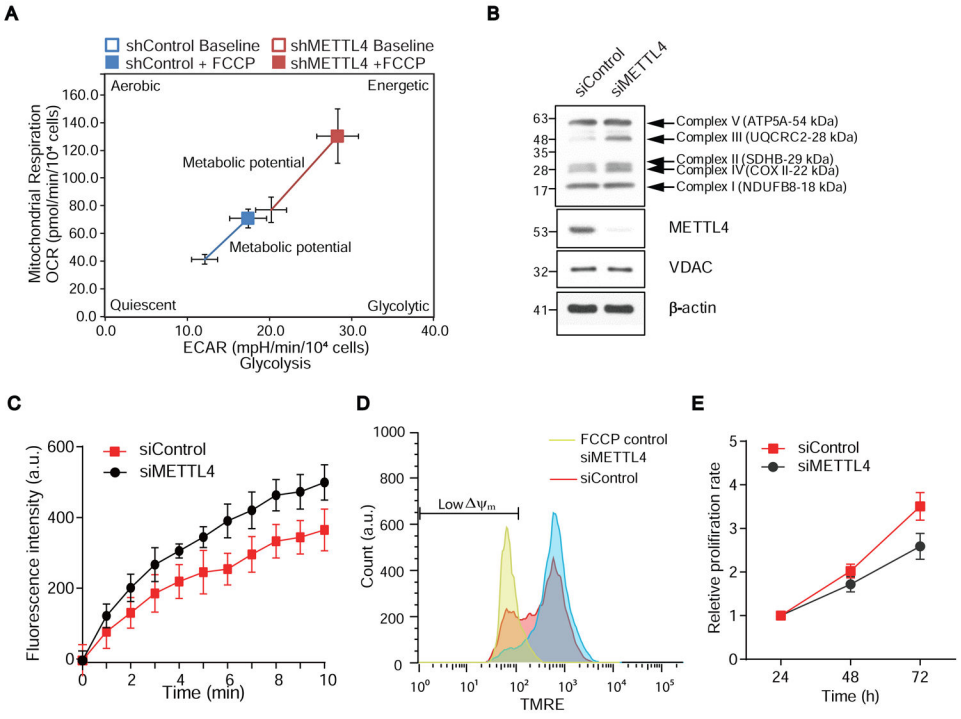

Figure 4. METTL4-mediated N^6-deoxyadenosine Methylation Affects Mitochondrial Functions

(A) Metabolic phenotype plot of oxygen consumption rate (OCR) vs. extracellular acidification rate (ECAR). METTL4 knockdown increased mitochondrial activity under both basal and stressed conditions (n = 4, mean ± SEM).

(B) METTL4 knockdown significantly increased OXPHOS complex III assembly and complex IV was also shown slightly increased.

(C) METTL4 knockdown increased ROS generation in mitochondria (n = 8, mean ± SEM).

(D) METTL4 knockdown increased the overall membrane potential of mitochondria.

(E) METTL4 knockdown decreased cell proliferation rates (n = 5, mean ± SEM).

See also Figure S4.

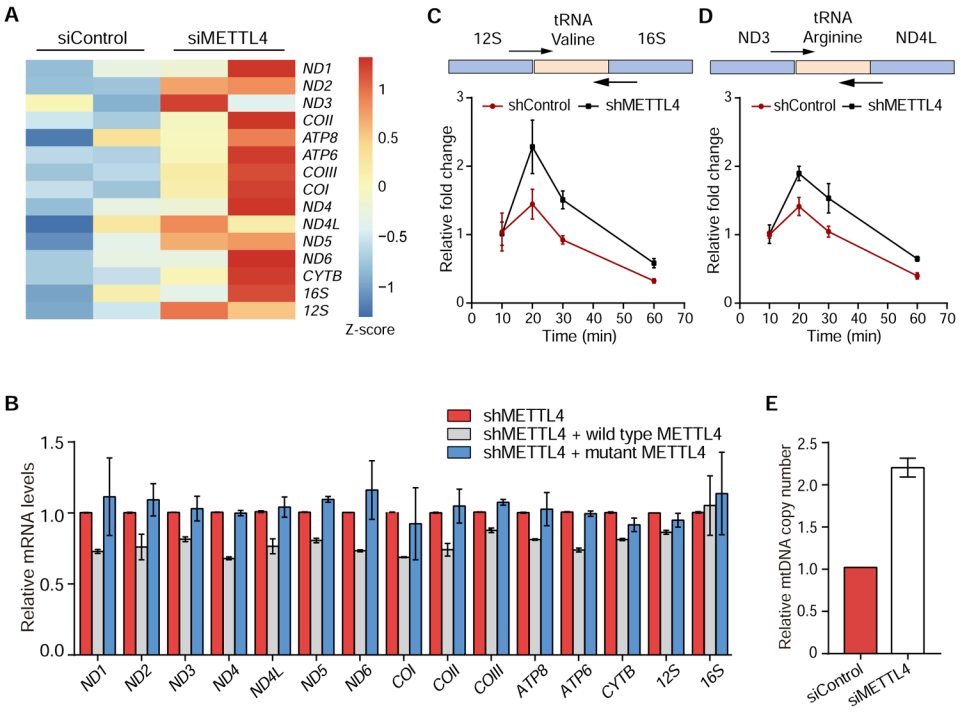

Figure 5. METTL4-mediated N^6-Deoxyadenosine Methylation Affects Levels of Mitochondrial Transcripts and Mitochondrial DNA (mtDNA) Copy Number

(A) Heatmap summarizing the mtDNA encoded transcripts from RNA-seq analysis. METTL4 knockdown increased the expression level of most mtDNA encoded mRNAs and rRNA.

(B) METTL4 knockdown and complementation showed that the methylation activity of METTL4 contributes to mitochondrial gene expression regulation (n = 3, mean ± SEM).

(C) - (D) Fold change of mitochondrial precursor RNA transcripts in the control and METTL4 knockdown cells at different time points after EU labeling. Primers for qPCR were designed for mt-tRNA^{Val} (C) and mt-tRNA^{Arg} (D) junction sites (n = 4, mean ± SEM). METTL4 knockdown increases the formation rate of mitochondrial precursor RNA.

(E) METTL4 knockdown doubled the relative mtDNA copy number (n = 3, mean ± SEM). See also Figure S5.

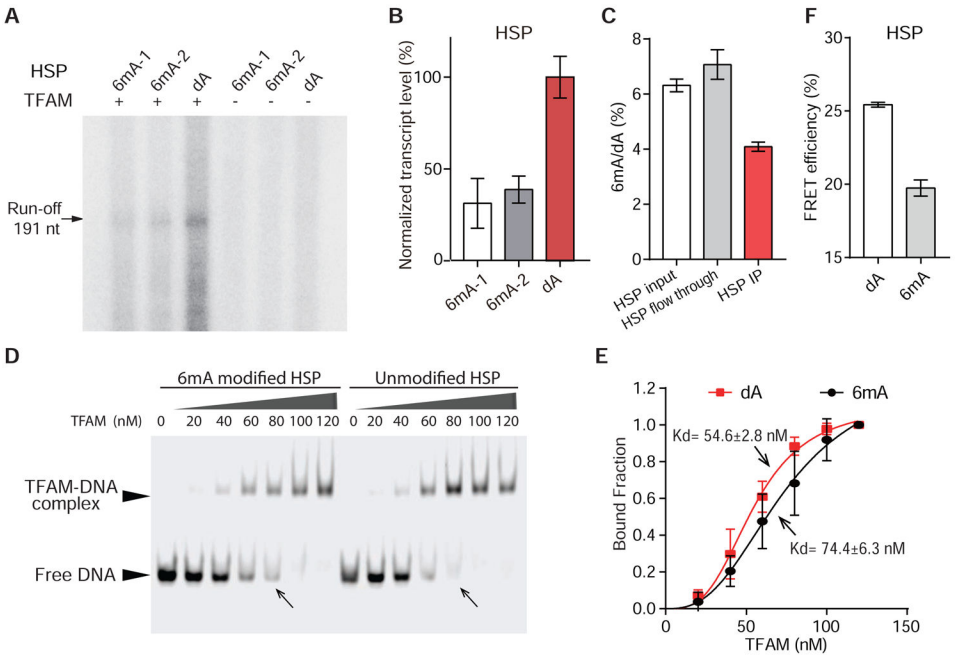

Figure 6. DNA 6mA Methylation Attenuates Mitochondrial Transcription and Affects Binding/Bending of DNA by TFAM

(A) *In vitro* transcription assays showing that 6mA suppresses transcription derived from the HSP promoter.

(B) Quantification of transcript levels in 6mA-modified and unmodified HSP probes. The level of transcript from the 6mA-modified probes were normalized to that from the unmodified probe (n = 2, mean ± s.d.).

(C) *In vitro* competition assays showing that the ratio of 6mA/dA was depleted in the TFAM-IP fraction while enriched in the flow-through fraction (n = 2, mean ± s.d.).

(D) EMSA performed using the 6mA-modified and unmodified HSP probes with different concentrations of the TFAM protein.

(E) The dissociation constant of TFAM to the 6mA-modified and unmodified HSP probes were calculated from the plot of fraction bound as a function of the TFAM concentration (n = 2, mean ± s.d.).

(F) FRET efficiency of the 6mA-modified and unmodified HSP probes upon TFAM binding (n = 2, mean ± s.d.).

See also Figure S5.

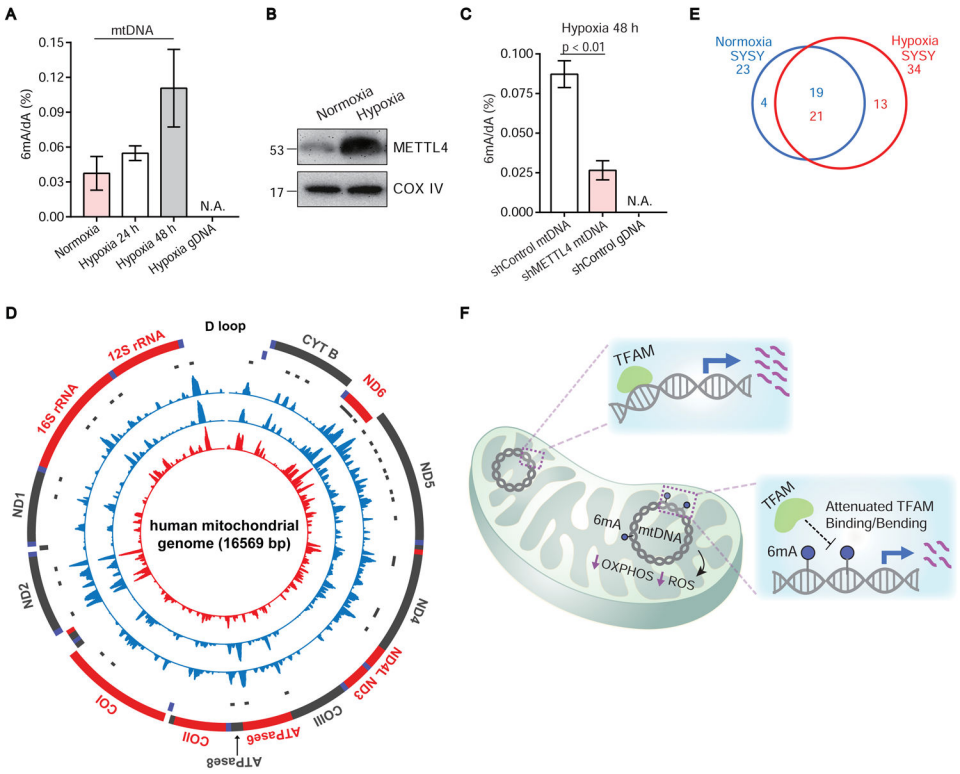

Figure 7. The Accumulation of METTL4-mediated 6mA Methylation in Mitochondria Under Hypoxic Stress

(A) The 6mA level in mtDNA increased during hypoxia treatment. Low 6mA was observed in gDNA under hypoxia ($n = 3$, $p < 0.01$, t test, mean ± SEM).

(B) The METTL4 protein level in mitochondria was elevated by ~2.5 fold under hypoxia.

(C) Knockdown of METTL4 under hypoxia resulted in a substantially reduced 6mA level in mtDNA ($n = 2$, $p < 0.01$, t test, mean ± SEM).

(D) Distributions of 6mA in mtDNA under hypoxia revealed by 6mA mapping. The mitochondrial genome is shown as the outermost circle in red/gray/blue with gene annotations. 6mA profiles revealed by SYSY-IP rep-1 (blue), SYSY-IP rep-2 (blue), and NEB-IP (red) were show in three tracks, respectively, from outside to inside. Gray dots and bars indicate 6mA peaks. Reads from input libraries have been subtracted.

(E) Peak overlap between 6mA mapping results under normoxia and hypoxia. 21 6mA peaks under hypoxia (certain peaks are broader under hypoxia) overlap with 19 peaks under normoxia.

(F) A schematic model showing mtDNA 6mA affecting mitochondrial functions.

See also Figure S6.

KEY RESOURCES TABLE

REAGENT or RESOURCE	SOURCE	IDENTIFIER
Antibodies		
Anti-METTL4 antibody	Sigma-Aldrich	Cat # HPA040061, RRID:AB_10697713
METTL4 Antibody (C-term)	Abgent	Cat # AP10377b, RRID:AB_10821964
Anti-m6A antibody	Synaptic Systems	Cat # 202 003, RRID:AB_2279214
Anti-m6A antibody	NEB	Cat # E1610S
VDAC (D73D12) Rabbit mAb(HRP Conjugate) antibody	Cell Signaling Technology	Cat # 12454, RRID:AB_2797922
Total OXPHOS Human WB Antibody Cocktail Kit	Abcam	Cat # ab110411, RRID:AB_2756818
mtTFA antibody	Abcam	Cat # ab119684, RRID:AB_10900340
SDHA Antibody	Cell Signaling Technology	Cat # 5839, RRID:AB_10707493
Mouse Anti-HIF-1 alpha Monoclonal Antibody	BD Biosciences	Cat # 610959, RRID:AB_398272
beta Actin antibody	GeneTex	Cat # GTX629630, RRID:AB_2728646
COX IV (4D11-B3-E8) Mouse mAb antibody	Cell Signaling Technology	Cat # 11967, RRID:AB_2797784
HDAC1 (10E2) Mouse mAb (HRP Conjugate) antibody	Cell Signaling Technology	Cat # 59581, RRID:AB_2799568
Chemicals, Peptides, and Recombinant Proteins		
MitoTracker Deep Red FM	Thermo Fisher	M22426
MitoTracker Red CM-H2XROS	Thermo Fisher	M7513
Nuclease P1	Wako USA	145-08221
Phosphodiesterase I from crotalus adamanteus venom	Sigma-Aldrich	P3243-1VL
FastAP Thermosensitive Alkaline Phosphatase	Thermo Fisher	EF0651
Tetramethylrhodamine, ethyl ester (TMRE)	Thermo Fisher	T669
5-ethynyl uridine (5-EU)	Thermo Fisher	E10345
(RS)-S-Adenosyl-L-methionine-d3 (S-methyl-d3) Tetra(p-toluenesulfonate) Salt	Central Chemicals Co., Inc.	D-4093
Recombinant HIV Reverse Transcriptase	Worthington	LS05003
Recombinant METTL4	This Study	N/A
Recombinant His-tagged TFAM	This Study	N/A
Human POLRMT (h-mtRNAP)	Enzymax	Cat. #: 81
Human TFAM (h-mtTFA)	Enzymax	Cat. #: 82
Human TFB2M (h-mtTFB2)	Enzymax	Cat. #: 83
Critical Commercial Assays		
Mitochondria Isolation kit	Miltenyi Biotec	130-094-532
Seahorse XFp Cell Energy Phenotype Test Kit	Agilent	103275-100
Click-iT® Nascent RNA Capture Kit	Thermo Fisher	C10365
TruSeq stranded mRNA sample preparation kit	Illumina	Cat. #: RS-122-2101
Deposited Data		
Raw and analyzed data	This paper	GEO: GSE102670
Imaging data	This paper	DOI: 10.17632/6byrgvmc59.1
Experimental Models: Cell Lines		

REAGENT or RESOURCE	SOURCE	IDENTIFIER
HeLa cell line	ATCC	Cat # CCL-2, RRID:CVCL_0030
HepG2 cell	ATCC	Cat # HB-8065, RRID:CVCL_0027
MDA-MB-231 Cell	ATCC	Cat # HTB-26, RRID:CVCL_0062
HEK293T Cell	ATCC	Cat # CRL-3216, RRID:CVCL_0063
143B cells	Yau-Huei Wei Lab	N/A
Rho zero 143B cells	Yau-Huei Wei Lab	N/A
Experimental Models: Organisms/Strains		
Primary fibroblasts	This Study	N/A
Mouse Brain	The Jackson Laboratory	C57BL/6J
Mouse liver	The Jackson Laboratory	C57BL/6J
Mouse testis	The Jackson Laboratory	C57BL/6J
Mouse heart	The Jackson Laboratory	C57BL/6J
Mouse fat	The Jackson Laboratory	C57BL/6J
Oligonucleotides		
siRNA for METTL4. Target sequence: AAGCCCTACGAAGGTATTATA	Qiagen	SI04136671
Primers for qPCR, see Table S2	This Study	N/A
Synthetic DNA probes, see Table S6	This Study	N/A
Recombinant DNA		
pHA-HIF-1α(ΔODD)	L. Eric Huang Lab	N/A
METTL4 MISSION shRNA shRNA Plasmid DNA	Merck	TRCN0000034831
pCMVΔR8.91	National RNAi Core Facility of Academia Sinica (Taipei, Taiwan)	N/A
pMD.G	National RNAi Core Facility of Academia Sinica (Taipei, Taiwan)	N/A
pCDH-CMV-METTL4-T2A copGFP	This study	N/A
pET28a-TFAM-SUMO-His_6	This Study	N/A
Software and Algorithms		
ImageJ		https://imagej.nih.gov/ij/
Gaphad Prism 7	California corporation	https://graphpad-prism.software.informer.com/7.0/
Hisat software		http://www.ccb.jhu.edu/software/hisat/index.shtml
Tophat		https://ccb.jhu.edu/software/tophat/index.shtml
rMATS (version 4.0.2)		http://rnaseq-mats.sourceforge.net/
Bowtie2		http://bowtie-bio.sourceforge.net/bowtie2/index.shtml
FeatureCounts		http://subread.sourceforge.net/